Journal of Structural Geology 140 (2020) 104139

Contents lists available at ScienceDirect

Journal of Structural Geology

journal homepage: http://www.elsevier.com/locate/jsg

Shear zone evolution during core complex exhumation – Implications for continental detachments

J.D. Wiest [a,*], H. Fossen [a,b], J. Jacobs [a]

[a] Department of Earth Science, University of Bergen, P.O. Box 7803, 5020, Bergen, Norway
[b] Museum of Natural History and Department of Earth Science, University of Bergen, P.O. Box 7803, 5020, Bergen, Norway

ARTICLE INFO

Keywords:
Caledonian post-orogenic collapse
Metamorphic core complexes
Ductile-to-brittle deformation
Rheological weakening
Phyllosilicates

ABSTRACT

The formation of low-angle detachments involves exhumation of previously ductile material and fault zone weakening. To better understand this relationship, we studied a deeply eroded metamorphic core complex, which formed in the core of the Bergen Arcs (W Norway) during Caledonian post-orogenic collapse. Multi-scale structural mapping in the Øygarden Complex constrains three structural levels characterized by localized shear (Upper Unit), distributed deformation (Middle Unit) and a migmatite double-dome (Lower Unit). All levels show retrogressive E-W stretching accompanied by extension-parallel recumbent folding, albeit, with opposing shear senses at upper and middle/lower levels. The systematic comparison of 23 shear zones constrains the ductile-to-brittle structural evolution. Initially, high temperatures and partial melting controlled pervasive deep crustal flow and ductile doming. During retrogressive shearing, lithological heterogeneity controlled strain localization and channelized fluid flow causing retrograde phyllosilicate growth. This established a feedback loop of fluid-flow, fabric weakening and progressive shear localization. The interconnection of inherited and newly formed weak, phyllosilicate-rich layers promoted the formation of bivergent detachments that rapidly exhumed a dome of previously ductile crust. Retrogressive weakening in a kilometer-wide ductile-to-brittle 'processing zone' may be essential for the formation of continental detachments.

1. Introduction

Detachments are ductile-to-brittle low-angle normal faults (Fig. 1) that record commonly 10s of kilometers of displacement (Armstrong, 1972; Axen, 2007; Buck, 1988; Lister and Davis, 1989; Wernicke, 1981). While oceanic detachments form at (ultra)slow spreading ridges (Fig. 1d), continental detachments are found in convergent as well as divergent tectonic settings (Platt et al., 2015; Whitney et al., 2013). Syn-convergent continental detachments (Fig. 1a, e g. South Tibetan Detachment) can form through (episodic) gravitational collapse (Burchfiel and Royden, 1985; Rey et al., 2001; Zhang et al., 2012) or channel flow and ductile extrusion (Beaumont et al., 2001; Grujic et al., 1996; Searle, 2010; Teyssier et al., 2005; Vannay and Grasemann, 2001). Classical low-angle detachments in the North American Cordillera, on the other hand, result from large-magnitude extension and bound domes/antiforms of metamorphic rocks known as metamorphic core complexes (MCCs; Fig. 1b) (Armstrong, 1982; Coney, 1980). Similar structures are found around the globe, particularly in areas that experienced orogenic collapse such as the Aegean (Jolivet and Brun, 2010), Variscides (Vanderhaeghe et al., 2020) or Caledonides (Fossen, 2010). Furthermore, recent models of passive margins increasingly invoke a crucial role of detachments and supradetachment basins in their distal parts (Fig. 1c; Brun et al., 2018; Clerc et al., 2018; Jolivet et al., 2018; Osmundsen and Péron-Pinvidic, 2018).

Although detachments are fundamental tectonic features, their formation is far from fully understood (Axen, 2007). Driving forces, low-angle fault mechanics, localization mechanisms and structural models are often controversial (Labrousse et al., 2016; Lavier et al., 1999; Platt et al., 2015; Searle and Lamont, 2020). Detachments in distinct lithospheres, settings and areas clearly have different characteristics (John and Cheadle, 2013), still their formation shows two common denominators: I) Detachments are inevitably associated with the exhumation of previously ductile material (Fig. 1), sometimes including (partially) molten rocks (Whitney et al., 2013); II) Detachment faults are weakened by growth of weak phases such as phyllosilicates (Collettini et al., 2009b; Grasemann and Tschegg, 2012; Holdsworth, 2004). Therefore, the retrogressive structural and rheological evolution of the ductile crust is a key to better understand the formation of

* Corresponding author.
E-mail address: johannes.wiest@uib.no (J.D. Wiest).

https://doi.org/10.1016/j.jsg.2020.104139
Received 20 November 2019; Received in revised form 2 July 2020; Accepted 6 July 2020
Available online 3 August 2020

detachment zones. However, even in exposed continental detachment systems, inadequate erosion levels or steep topographic relief (Fig. 1) often limit access to systematically study their ductile parts.

To address this issue, we studied the deeply eroded footwall of a major continental detachment system in W Norway that formed during collapse of the Caledonian orogen (Andersen and Jamtveit, 1990; Fossen, 2010; McClay et al., 1986; Norton, 1987; Osmundsen et al., 2005). Located in the core of the Bergen Arcs megastructure (Fig. 2), the Øygarden Complex (ØC) represents a domiform MCC with a flat erosion surface at sea level (Fig. 3) that cuts through ~10 km of crustal section. The so-called 'strandflat' morphology (Holtedahl, 1998) results in >1200 km of coastlines within an area of 75 km × 25 km, furthermore complemented by road sections along and across structural trends. This situation provides ideal conditions for systematic structural mapping at multiple scales. In this contribution, we present the first comprehensive study of ductile(-to-brittle) structures in the ØC including semi-quantitative mapping of ductile strain with the DISK scheme (Wiest et al., 2019) and a systematic analysis of 23 shear zones. Based on our results, we discuss the boundary conditions and dynamics of MCC formation and the structural evolution of the exhuming ductile crust. We compare the ØC to MCCs in other orogens, neighboring domes, and geodynamic models, to infer implications for the formation of large-magnitude continental detachments.

1.1. Detachments vs. décollements

Although the term detachment is sometimes also used to include reverse faults or thrust zones with marked structural and/or metamorphic breaks (e.g. Milnes et al., 1997), we here follow Whitney et al. (2013) and restrict the term to large-magnitude, low-angle, extensional high-strain zones that comprise ductile shear zones as well as brittle faults. As pointed out by Brun et al. (2018), the terms detachment and décollement are not synonymous. Detachments are kilometer-scale fault zones, which cut across lithological contacts and unit boundaries (incision and excision as defined by Lister and Davis, 1989). In contrast, décollements are weak layer-parallel horizons localizing deformation, which can occur from the microscale (see examples below) to the scale of entire orogens (Fossen, 1992).

2. Geological setting

The Øygarden Complex (ØC) is a dome-shaped window (Fig. 3) that exposes Baltic Shield basement in the core of the Bergen Arcs (Kolderup and Kolderup, 1940). The latter is an enigmatic megascale structure that formed through the combined effects of Caledonian orogenesis and post-orogenic collapse (Fossen and Dunlap, 1998).

2.1. Baltic Shield

The Baltic Shield in W Norway originally formed between 1.6 and 1.5 Ga through arc magmatism and sedimentation (Bingen and Solli, 2009; Roberts and Slagstad, 2015; Roberts et al., 2013). The crustal configuration of this part of the Baltic Shield mainly formed during the 1.2–0.9 Ga Sveconorwegian orogeny (Bingen et al., 2005). Alternating episodes of extension and contraction characterized by a hot orogenic setting (Bingen et al., 2008) involved extensive magmatism and widespread migmatization (Coint et al., 2015; Slagstad et al., 2013, 2018b). During the Ediacaran, a segmented passive margin was established and continental ribbons rifted off the margin while the Iapetus ocean was opened (Andersen et al., 2012; Jakob et al., 2019; Kjøll et al., 2019). The Baltic Shield was transgressed and Cambrian shales were deposited onto deeply eroded Sveconorwegian crust (Gee et al., 2008).

2.2. Caledonian orogeny and extensional collapse

The Silurian to Early Devonian Caledonian orogeny comprises the closure of the Iapetus ocean until collision of Baltica (lower plate) with Laurentia (upper plate) from around 430 Ma (Corfu et al., 2014; Slagstad and Kirkland, 2018). Nappe stacking of different units of the Iapetus ocean, the Laurentian margin and the previously formed continental ribbons formed a thick orogenic wedge that was thrusted onto the Baltican margin while the Cambrian shales acted as a basal décollement (Fossen et al., 2017; Gee et al., 2008). At this stage, the Baltican margin must have been very strong so that it could get coherently subducted (Butler et al., 2015) reaching high-to ultrahigh-pressure conditions recorded in eclogites (ages ~425–400 Ma, see compilation by Kylander-Clark and Hacker (2014)) and felsic gneisses in the Western Gneiss Region/Complex (Cuthbert et al., 2000; Dobrzhinetskaya et al., 1995;

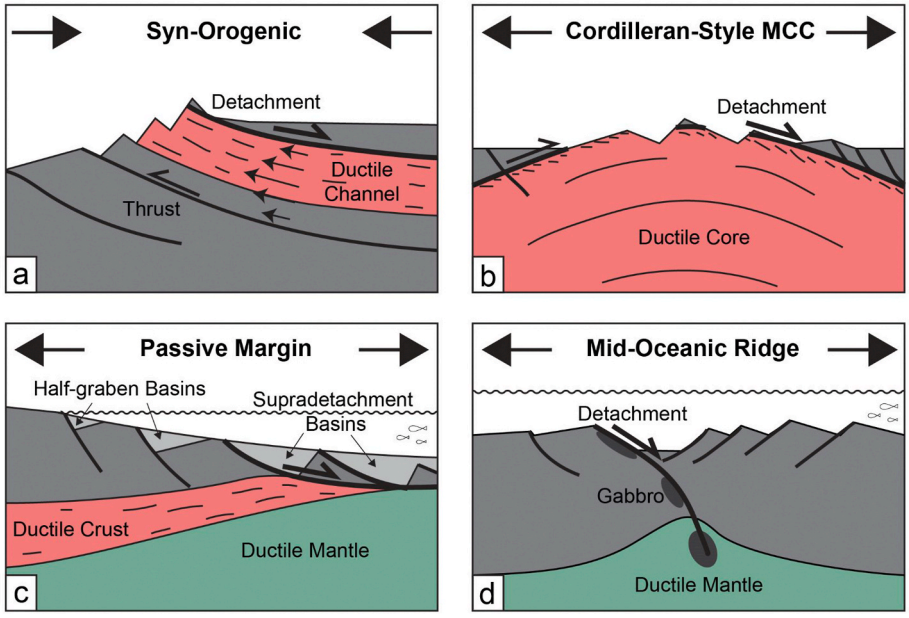

Fig. 1. Cartoon-style cross sections of detachments in different tectonic settings. In all cases their formation is linked to exhumation of previously ductile material, but the systematic study of ductile footwalls is commonly inhibited by steep relief, erosion level or water cover. Loosely based on: a: Beaumont et al. (2001); b: Miller et al. (1999); c: Clerc et al. (2018); d: Whitney et al. (2013).

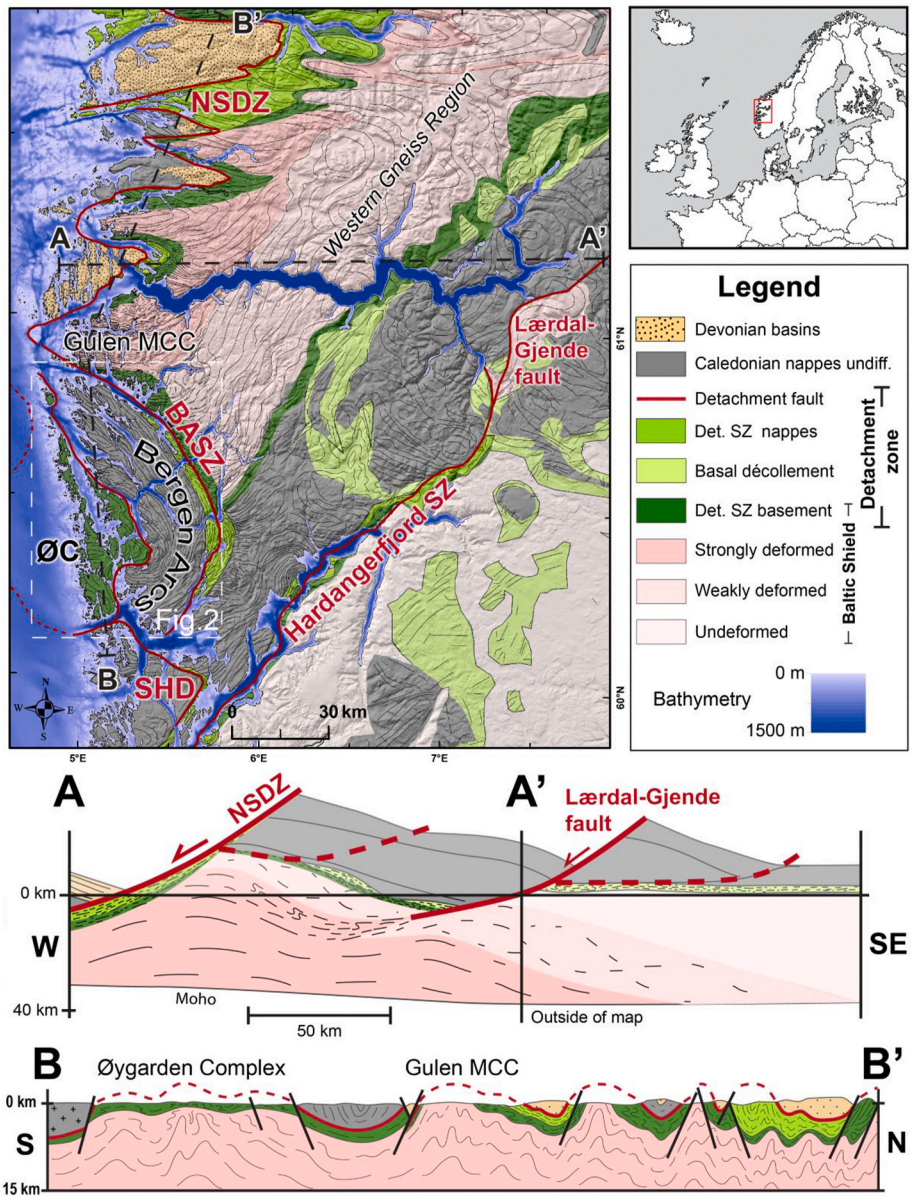

Fig. 2. Regional tectonic map of W Norway, showing brittle and ductile features of the Devonian detachment system and the intensity of (post-orogenic) Caledonian deformation in the Baltic Shield basement. The Øygarden Complex (ØC) represents a basement window affected by detachment shearing. The E-W cross-section A-A' (modified from Milnes et al., 1997) shows exhumation of strongly deformed basement below the Nordfjord-Sogn detachment zone (NSDZ) and Devonian supradetachment basins. The N–S cross section B–B' (modified from Johnston et al., 2007b; Krabbendam and Dewey, 1998; Wiest et al., 2019) shows the relation between the corrugated detachment and extension-parallel basement domes, including the ØC and the Gulen MCC. A white rectangle marks the location of Fig. 2. Other abbreviations: BASZ – Bergen Arcs shear zone, SHD – Sunnhordland detachment.

Griffin and Brueckner, 1980; Root et al., 2005; Wain, 1997).

While there is evidence for syn-convergent detachments in the overriding plate on the Laurentian (Greenland) side of the orogen (Andresen et al., 2007; Hartz et al., 2001; Hodges, 2016), the Scandinavian lower plate shows overwhelming evidence for post-orogenic collapse (Fossen, 1992, 2010). Following continent collision from around 405 Ma, reversed plate movements (Fossen et al., 2017; Rey et al., 1997) led to extensional reactivation of the basal décollement (Fossen, 2000) and the resulting eduction of the continental slab caused near-isothermal decompression of the deeply buried Baltican crust (Andersen et al., 1991; Butler et al., 2013; Duretz et al., 2012; Root et al., 2005). Crystallization ages of migmatites between 405 and 390 Ma witness the thermal softening and increased buoyancy of the orogenic root at this stage (Ganzhorn et al., 2014; Gordon et al., 2013; Kylander-Clark and Hacker, 2014; Labrousse et al., 2002). This led to wholesale collapse of the overthickened crust in a regime of sinistral transtension, forming orogen-scale extensional detachments and sinistral strike-slip zones while Devonian supradetachment basins were deposited (Andersen and Jamtveit, 1990; Chauvet and Seranne, 1994; Fossen, 2010; Fossen et al., 2013; Hossack, 1984; Krabbendam and Dewey, 1998; Osmundsen and Andersen, 2001; Osmundsen et al., 2006; Séguret et al., 1989; Seranne, 1992; Seranne and Seguret, 1987). Ages of amphibolite-to greenschist-facies reworking during exhumation and cooling mostly fall between 405 and 375 Ma (Chauvet and Dallmeyer, 1992; Fossen and Dallmeyer, 1998; Fossen and Dunlap, 1998; Kylander-Clark et al., 2008; Spencer et al., 2013; Walsh et al., 2013).

Post-orogenic deformation shows a regional strain gradient from cold crust in the foreland and the upper parts of the orogenic wedge to hot crust in the orogenic infrastructure (Fauconnier et al., 2014; Fossen et al., 2014; Hacker et al., 2010; Milnes et al., 1997). The Hardangerfjord shear zone (Fig. 2) is an extensional shear zone that cross-cuts the basal décollement and corresponds to the limit of thick-skinned post-orogenic deformation involving the Baltic Shield basement (Fossen and Hurich, 2005). Along the west coast of southern Norway, the Nordfjord-Sogn detachment zone exhumed strongly deformed eclogite-bearing crust in MCCs that were juxtaposed with Devonian supradetachment basins (Braathen et al., 2004; Hacker et al., 2003b; Johnston et al., 2007a; Norton, 1987; Osmundsen and Andersen, 2001; Wiest et al., 2019). Deep crustal flow was largely coaxial (Andersen et al., 1994; Hacker et al., 2010) and involved large-scale internal necking as well as

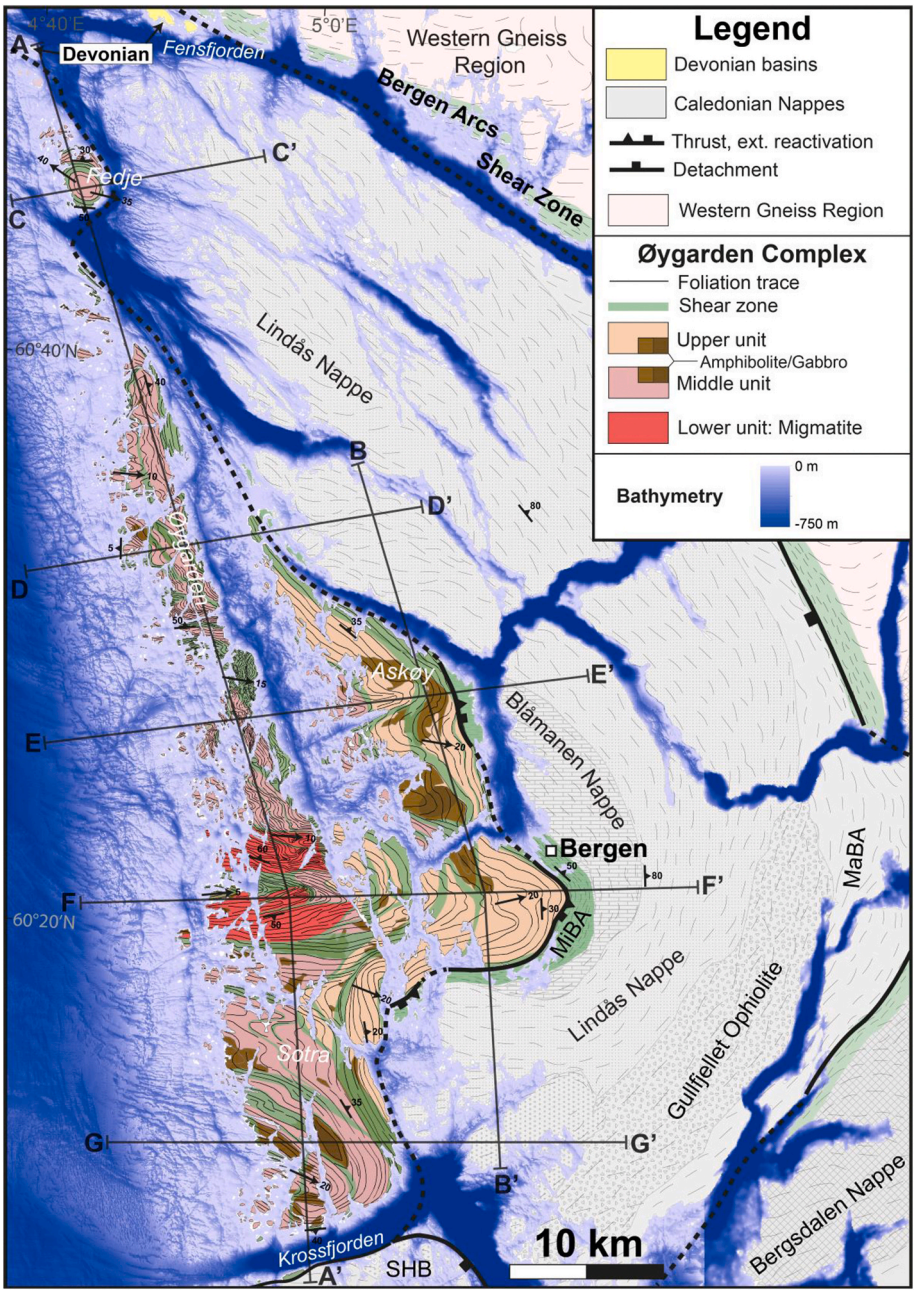

Fig. 3. New geological map of the Øygarden Complex distinguishing three map units (see section 3.1). Note that mafic bodies are contained in all of the units. Small remnants of Devonian supradetachment basins are exposed in the NW corner of the map. Steep brittle faults are not shown. Abbreviations: MaBA – Major Bergen Arc, MiBA – Minor Bergen Arc, SHB – Sunnhordland Batholith.

extension-parallel upright folding due to constriction (Fig. 2: cross section B–B''; Krabbendam and Dewey, 1998; Labrousse et al., 2002; Labrousse et al., 2004). In proximity to the detachment zones, coaxial flow was overprinted by retrograde simple-shear deformation that involved vertical shortening (Andersen et al., 1994; Johnston et al., 2007b; Wiest et al., 2019). Detachment shearing started at amphibolite-facies conditions and evolved progressively into brittle conditions (Braathen et al., 2004). From the Permian through the Mesozoic, two phases of North Sea rifting brittlely overprinted and partly reactivated Caledonian structures (Fazlikhani et al., 2017; Lenhart et al., 2019).

2.3. The Bergen Arcs

The Bergen Arc system (Fig. 3) consists of a heterogeneous stack of thrust nappes that were imbricated during Caledonian convergence (Kolderup and Kolderup, 1940; Kvale, 1960). The Minor Bergen Arc comprises elements of the Iapetus ocean (Fossen, 1989), while the Blåmanen Nappe represents a fragment of Baltican basement and its sedimentary cover (Fossen, 1988). The Lindås Nappe is famous for early Caledonian fluid-induced eclogitization of granulite-facies anorthosites and experienced partial melting leading to syn-convergent exhumation (Austrheim, 1987; Bingen et al., 2004; Jolivet et al., 2005; Kuhn et al., 2002; Labrousse et al., 2010). The Gullfjellet Ophiolite and the Sunnhordland Batholith belong to a suite of arc-related rocks that formed in a supra-subduction setting, possibly at the Laurentian margin (Andersen and Jansen, 1987; Furnes et al., 2012; Pedersen et al., 1992). The Major Bergen Arc includes parts of the pre-Caledonian hyperextended margin (Andersen et al., 2012; Jakob et al., 2017). Together, these different units are folded into an arcuate synformal structure, which occupies the

hanging wall of the extensional Bergen Arcs shear zone (Wennberg, 1996; Wennberg et al., 1998). The ØC forms the core of this structure and the contact between the ØC and the nappe stack is a basal thrust that has been reactivated as an antithetic detachment (Wiest et al., 2018b). Small remnants of Devonian supradetachment basins are preserved on islands directly north of the ØC (upper left corner of Fig. 3).

2.4. The Øygarden Complex (ØC)

The ØC consists of Telemarkian (1.5 Ga) granitic crust and Proterozoic metasediments that were migmatized and intruded by voluminous plutons during the ~1.0 Ga Sveconorwegian orogeny (Slagstad et al., 2018a; Sturt et al., 1975; Wiest, 2020; Wiest et al., 2018b; unpublished SIMS U–Pb zircon ages of granitic leucosomes). These 1050–1000 Ma Sveconorwegian magmatic rocks can be directly correlated with equivalent rocks in southern Norway, which are undeformed (Coint et al., 2015) and suggest an autochthonous position of the ØC and a Caledonian age of deformation (Wiest et al., 2018b). While large granitic and gabbroic plutons dominate the eastern and southern part of the complex (Askvik, 1971; Bering, 1985; Fossen and Ragnhildstveit, 2008; Weiss, 1977; Wiest et al., 2018b), the central and northern part comprise mostly migmatites, leucogranites and locally quartzite-schist assemblages that apparently resisted migmatization (Austrheim and Ragnhildstveit, 1999; Johns et al., 2001). Many of the granites in the entire ØC are exceptionally radioactive and associated with high heat production values (Pascal and Rudlang, 2016; Rudlang, 2011; Schulze, 2014). On the 1:250.000 geological map (Ragnhildstveit and Helliksen, 1997), mafic rocks cover 14% of the exposed surface of the ØC, but smaller scale mafic bodies are abundant.

During the Caledonian orogenic cycle, the ØC experienced intense ductile reworking (Fossen and Rykkelid, 1990; Rykkelid and Fossen, 1992) including partial melting of the lowest levels (Johns, 1981). SIMS U–Pb zircon ages date crystallization of granitic leucosomes at 405 ± 3 Ma and overlap with Ar–Ar white mica and biotite ages in between 405 and 399 Ma (Wiest, 2020). These new ages confirm that most of the observed deformation occurred during post-orogenic collapse and led to rapid exhumation of ductile crust as suggested by previous models (Boundy et al., 1996; Fossen and Dunlap, 1998; Fossen and Rykkelid, 1992; Wiest et al., 2018b). This is furthermore constrained by the onset of brittle faulting dated at ca. 396 Ma (Larsen et al., 2003). During North Sea rifting, the ØC formed a horst (Fossen, 1998) and limited number of coast-parallel alkaline dikes intruded in the Permian and Triassic (Fossen and Dunlap, 1999). Steep brittle faults, which cut through the gneissic fabrics, formed in multiple episodes from the Carboniferous until the Cretaceous (Fossen et al., 2016; Ksienzyk et al., 2014, 2016).

3. Structural architecture of the ØC

The ØC forms a shallow dome structure with only the eastern half exposed. The western part is below sea level and structural trends can be traced in the bathymetric data (Fig. 3). A series of cross-sections and a pseudo-3D view (Fig. 4) show the internal architecture of the complex. Extension-parallel E-W sections show consistently E-dipping fabrics that obtain a gentle westward dip at the westernmost exposures and in offshore seismic sections (Fossen, 1998; Grünwald, 1994). The ca. 25 km-long, continuously exposed central E-W section (F–F′) represents ca. 10 km of vertical crustal section from the top of the complex in the east to the deepest exposed levels in the west. Extension-perpendicular N–S sections show a very different picture. At upper levels (section B–B′), the gneissic fabric forms an open antiform with second-order undulations. At lower levels (section A-A'), the gneissic fabrics define five subdomes. Except for the Fedje dome (Larsen, 1996) in the north, the subdomes are exposed as E-plunging antiforms (Larsen et al., 2003). At the lowest level in the core of the complex, migmatites define a double-dome structure.

We distinguished three structural units within the ØC that are characterized in the following section 3.1. They share important

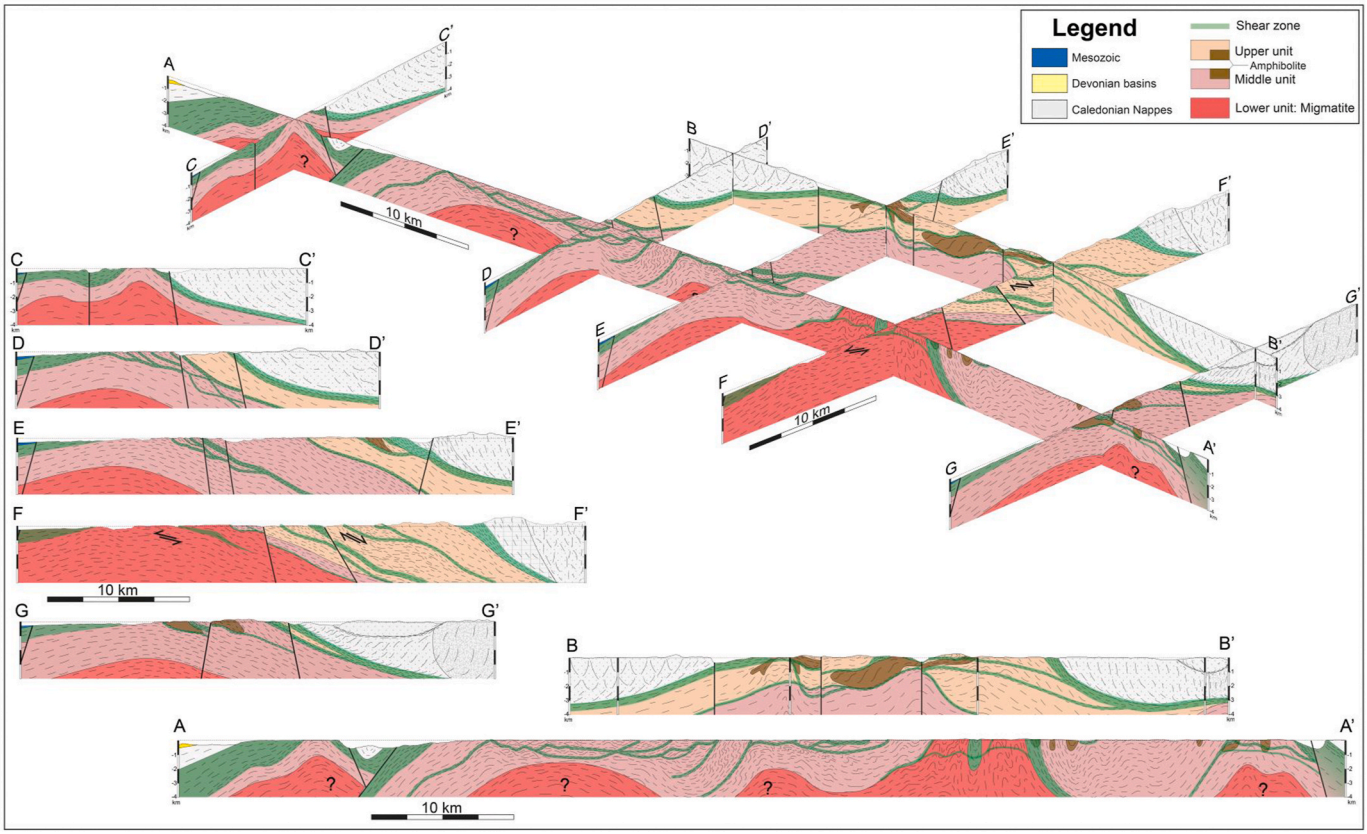

Fig. 4. Cross sections and pseudo-3D network of cross sections. See Fig. 2 for locations.

similarities such as retrogressive simple shearing, similar orientations of fabrics of different metamorphic grades (section 3.2) and a similar style of stretching and folding (3.3). Section 4 provides a more detailed characterization of shear-zone evolution in each of the units.

3.1. Structural units (levels)

3.1.1. Upper Unit

Localized amphibolite-facies deformation characterizes the Upper Unit (Fig. 5). Pervasive shearing was weak and dominated by L > S fabrics (Fig. 6) so that primary textures within large Precambrian granite and gabbro plutons were preserved (Wiest et al., 2018b). Augen gneisses with feldspar augen in a fine-grained multi-phase matrix represent the most common rock type. Banded gneisses and mylonites are only found in high-strain zones. Retrograde deformation at greenschist facies to semi-brittle conditions was abundant in the Upper Unit. On the map scale, there are large tracts of phyllonites and fault rocks that range from mixed mylonites/cataclasites to amorphous ultracataclasites. On the microscale, low-temperature/high-stress fabrics commonly overprint coarse-grained high-grade fabrics. Quartz-rich rocks show regime 3 fabrics as defined by Hirth and Tullis (1992), cut by micro-scale shear zones and mylonitic quartz veins with regime 1–2 fabrics (electronic supplement 2). While symmetric fabrics are sometimes found in homogeneous gneisses and amphibolites, most fabrics are asymmetric, especially where phyllosilicate-rich layers are present, and indicate almost exclusively top-to-E kinematics (Fig. 6).

3.1.2. Middle Unit

Pervasive amphibolite-facies shearing characterizes the Middle Unit (Fig. 5). It consists largely of banded gneisses and amphibolites, while Precambrian protoliths and localized deformation are only found in low-strain domains (Fig. 6). Isolated lenses of micaschist contain kyanite, sillimanite and garnet. The characteristic rock type of the unit are banded gneisses with L = S fabrics (Fig. 6) formed by a medium-grained phase mix of quartz, feldspar and biotite. Fine-grained feldspar layers show no competence contrast to quartz-rich layers with regime 3 microfabrics. Feldspar-rich pegmatites, on the other hand, represent weakly deformed rigid bodies within gneisses and amphibolites. Progressive strain-localization occurred during retrograde deformation from kilometer-scale gneissic zones into meter-scale high-strain zones. These weak zones are inherited micaschists or formed by retrograde, fluid-induced phyllonitization (see documentation in section 4.3 and electronic supplement 2). In either case they show highly localized semi-brittle deformation. On the microscale, regime 1–2 quartz microstructures are restricted to micro-scale shear zones, while the gneissic fabric shows abundant sericitization and saussuritization. Similar to the Upper Unit, coaxial deformation is recognized in homogeneous gneisses and amphibolites (Fig. 6), but more common are asymmetric fabrics

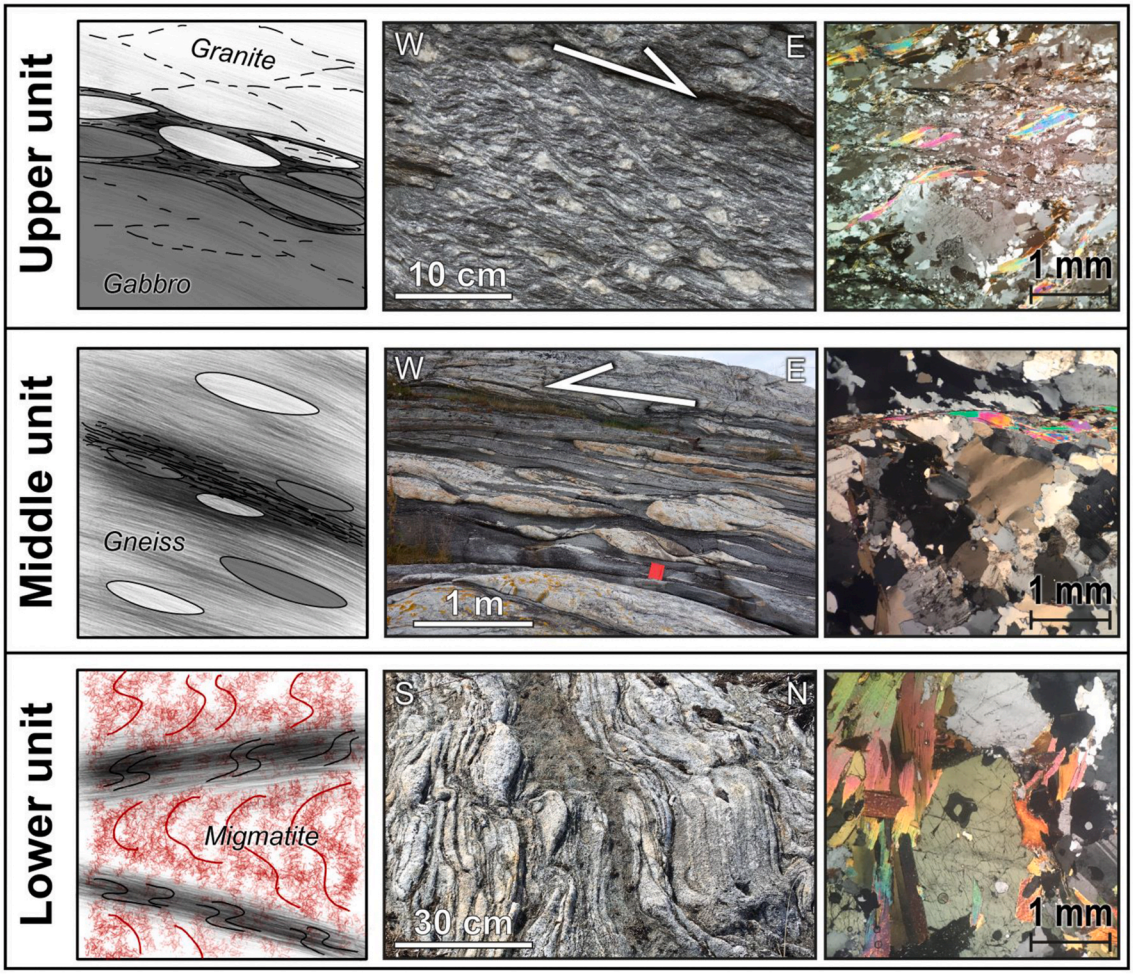

Fig. 5. Characteristics of the structural units: Localized deformation preserves protoliths in the Upper Unit. Most fabrics show top-to-E kinematics and pervasive low-grade deformation on the microscale. The Middle Unit comprises pervasively sheared gneisses with low-strain lenses preserving protoliths. Most fabrics show top-to-W kinematics and low-grade deformation is highly localized, even on the microscale (note muscovite growing in micro-shear zone). The Lower Unit consists of late Caledonian migmatite (Wiest et al., 2018a). Localized post-migmatitic shear zones transform the migmatites into banded gneisses, but large domains preserve magmatic (micro-)structures.

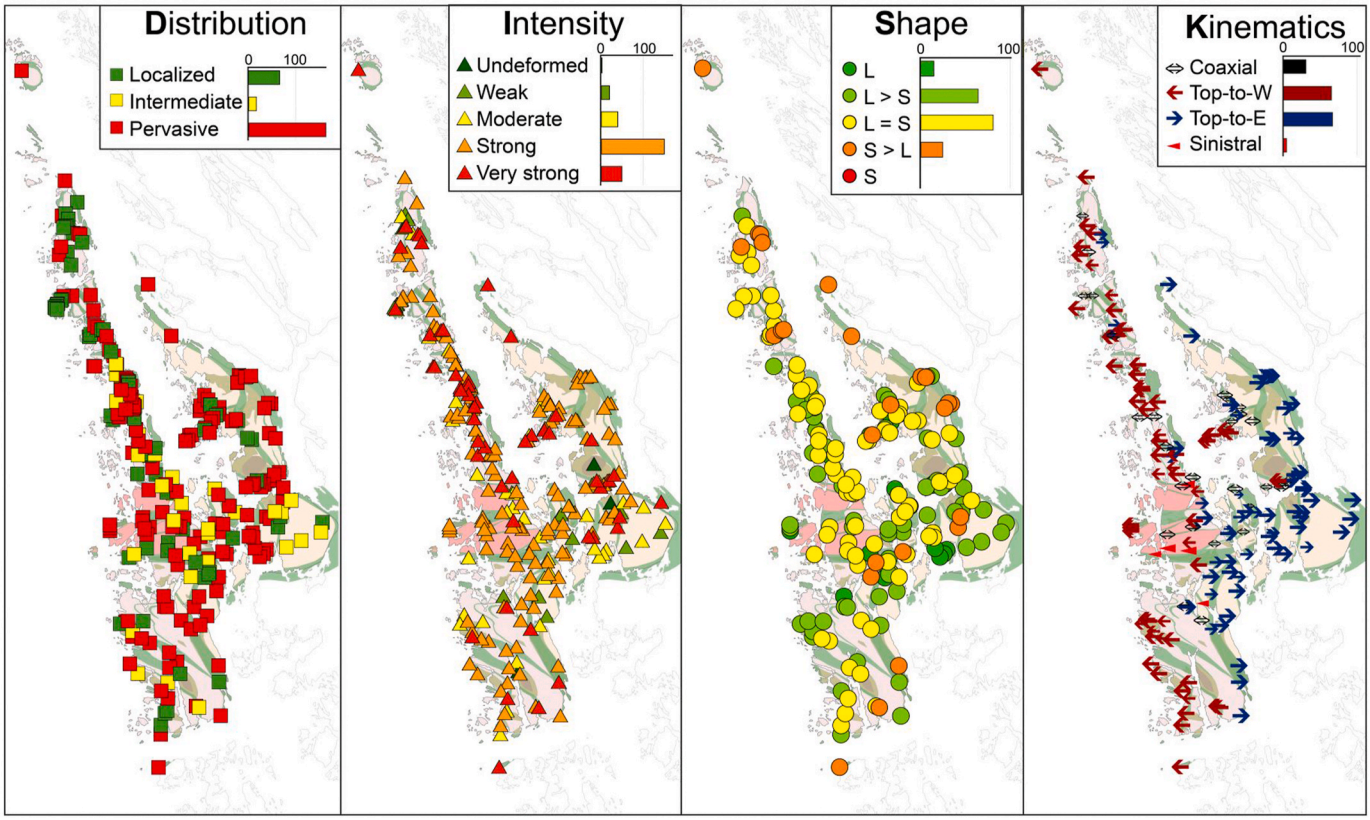

Fig. 6. Semi-quantitative mapping of ductile strain with the DISK scheme (Wiest et al., 2019). The results are shown separately for each parameter as map symbols and corresponding histograms. The symbols for kinematics are scaled corresponding to the confidence of the observation (small symbols – uncertain, middle symbols – certain, large symbols – very certain).

indicating top-to-W kinematics. Simple shearing comprises distributed as well as localized deformation at different metamorphic grades, ranging from banded gneisses to semi-brittle chlorite phyllonites (see section 4.3). The mapped boundary between Upper and Middle Unit (localized vs. distributed deformation) coincides with the respective occurrence of top-to-E and top-to-W fabrics.

3.1.3. Lower Unit

The Lower Unit (Fig. 5) consists of Caledonian migmatites with melt crystallization dated by SIMS U–Pb zircon geochronology to 405 ± 3 Ma (Wiest et al., 2018a). These migmatites are metatexites with varying amounts of melt and form a double-dome structure with steep E-W striking foliations in the core of the complex (Fig. 4). However, heterogeneous solid-state deformation overprinted the original geometry of the migmatite bodies. A weak pervasive stretching lineation developed in biotite-melanosomes, while localized shear transformed the migmatites into banded gneisses. A suite of garnet-staurolite-kyanite amphibolites within the migmatites show a progressive development from melt-present deformation to ductile-brittle greenschist facies deformation (see section 4.4). Other shear zones in the migmatite domain show a cataclastic overprint.

3.2. Fabric orientations

We compiled a large structural dataset, which comprises newly acquired data from this study, digitized measurements from structural maps (Bering, 1985; Bernhard, 1994; Grünwald, 1994; Johns, 1981; Larsen, 1996; Wiest et al., 2018b; Ytredal, 1995, 1996) as well as the digital structural database of maps from the Norwegian geological survey (Andersen et al., 1988; Austrheim and Ragnhildstveit, 1999; Bering et al., 1988; Fossen and Ragnhildstveit, 2008; Johns et al., 2001). In total, our dataset comprises 4024 foliations, 1072 lineations and 115 fold axes and is made available in electronic supplement 1.

Fabrics throughout the complex show a consistent pattern of shallowly ESE-plunging stretching lineations, lineation-parallel fold axes and a corresponding girdle of mostly flat-lying foliations (Fig. 7). Structural trends are similar in the three units and amphibolite- and greenschist-facies fabrics are parallel. The migmatitic Lower Unit, however, shows steeper migmatitic foliations cut by solid-state fabrics (electronic supplement 2). We distinguish six structural subareas to highlight second-order geographical variations in fabric orientations. The Laksevåg area (Upper Unit) shows a dominant ENE fabric trend that rotates towards ESE in the northern part of the Askøy area (Upper and Middle Unit) and in the southern Sotra area (Upper and Middle Unit). The Øygarden area (Middle Unit) shows consistently flat-lying foliations and an ESE-trend within a large scatter of linear fabrics. NE-plunging fold axes are found in weakly deformed rigid bodies. West-dipping fabrics occur in the westernmost part of this area. Linear fabrics in the Fedje area (Middle Unit) have a clear ESE-WNW trend, while foliations define a dome. Both linear and planar fabrics are here steeper than in most of the Middle and Upper Units. The migmatite core (Lower Unit) has steep migmatitic foliations that have been vertically shortened by solid-state shearing. The trend of fabrics in this area is close to E-W and foliations show a S-vergence with a steeper southern limb and a shallow northern limb. This asymmetry is reflected in the geometry of the entire complex (Fig. 3).

3.3. Folding and boudinage

Gneissic tectonites in the ØC are strongly anisotropic and display very different structural characteristics in lineation-parallel (E-W) and -perpendicular (N–S) sections (Fig. 8). Different fold structures are

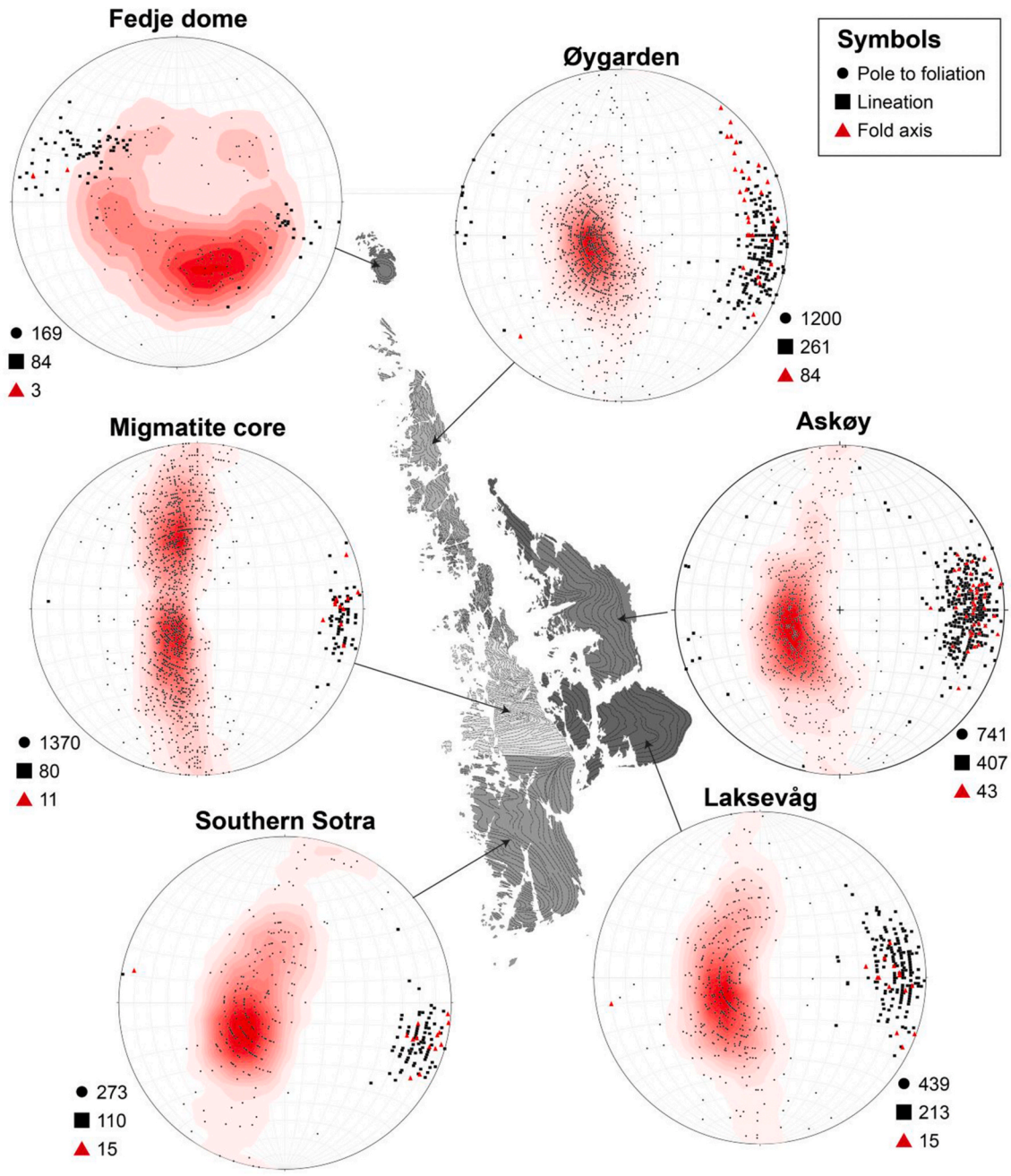

Fig. 7. Lower-hemisphere equal area plots of the compiled structural data grouped into six structural subareas. Poles to foliations (small black circles) are contoured in red. Note that some of the structural data digitized from maps was recorded only at 5° precision creating an unnatural scatter. See text for references. (For interpretation of the references to color in this figure legend, the reader is referred to the Web version of this article.)

observed on different scales. While E-W-trending upright folds are seen on the map-scale (Figs. 4 and 8a), tight to isoclinal recumbent folds are abundant on the outcrop-to micro-scale. Literal textbook examples of multilayer buckle folds (Fig. 8b; see Fossen, 2016) show that competent layers (amphibolites or feldspar-rich pegmatites) controlled fold geometries during vertical shortening. Fold hinges are commonly occupied by retrograded amphibolites (biotite ± chlorite phyllonites) in between more competent granitic layers (Fig. 8c). The weak phyllosilicate-rich layers allowed the formation of tight to isoclinal folds and show a genetic relationship between recumbent folds and retrogressive shear at amphibolite to greenschist facies conditions (see section 4).

In contrast to N–S sections, E-W sections show a remarkably parallel stratification of the undulating gneissic foliations (Fig. 8d). On the outcrop-scale, the lineation-parallel sections reveal abundant necking instabilities formed by layer-parallel extension. Purely ductile necking structures are symmetric, but more commonly we find asymmetric boudinage of amphibolites and feldspar-rich pegmatites associated with shear fractures (Fig. 8e). In heterogeneous gneisses, asymmetric foliation boudinage (Fig. 8f) and small-scale folding instabilities (Fig. 8g) formed above phyllosilicate-rich small-scale décollements (Rykkelid and Fossen, 1992). The map-scale structural relationships suggest that E-W stretching lead to necking and extension-perpendicular horizontal shortening forming upright folds. Under retrograde metamorphic conditions, shearing involved vertical shortening and was becoming progressively more non-coaxial.

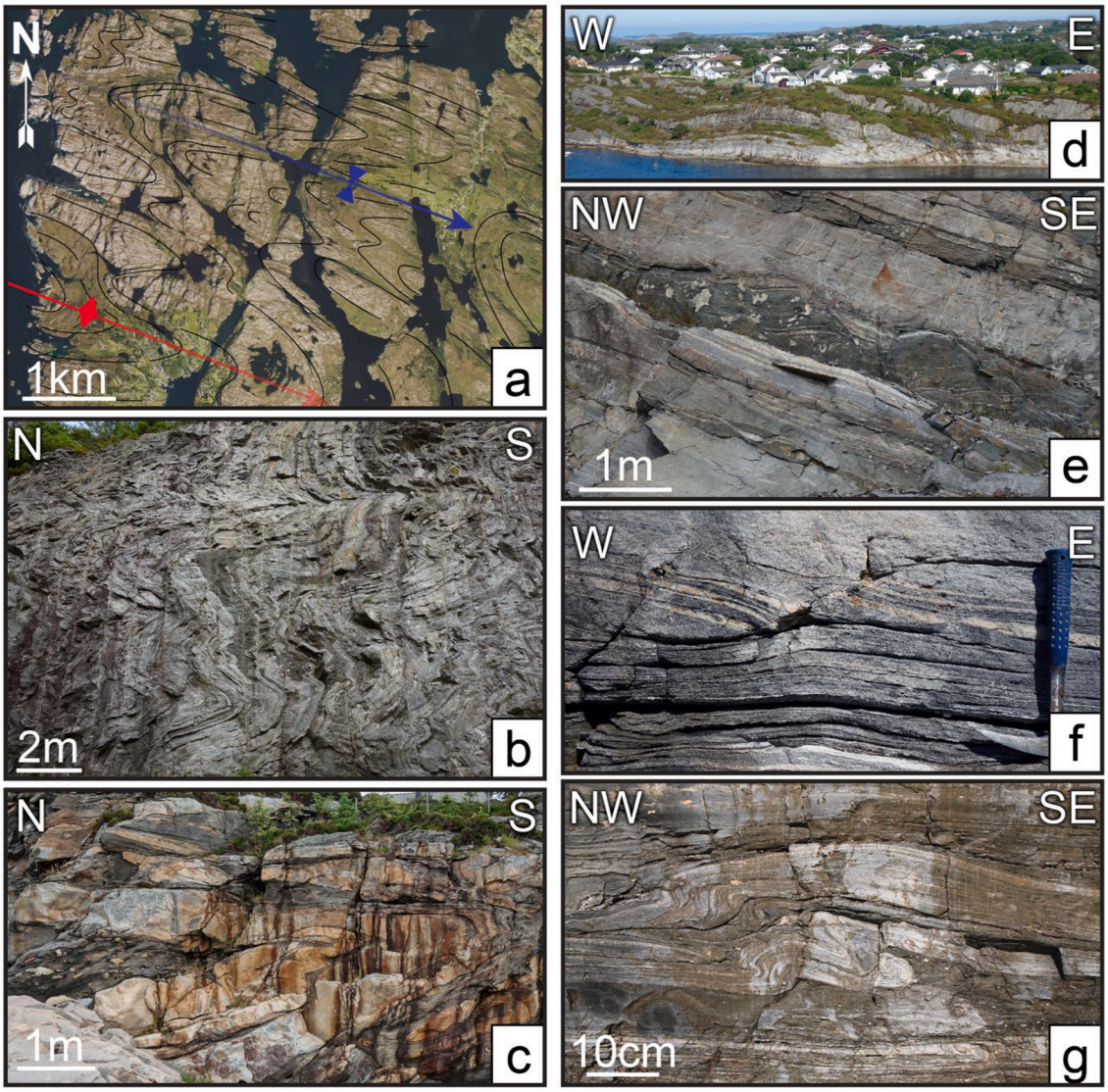

Fig. 8. Folding, stretching and boudinage. a: Kilometer-scale ESE-plunging antiform (red) – synform (blue) - pair on southern Sotra. Black lines highlight the trace of the foliation. Orthophoto from norgeskart.no. b: Multilayer buckle folds in heterogeneous gneiss of the Toftøy shear zone indicating vertical shortening. c: Granitic pegmatite folded into isoclinal recumbent fold in the Ramsøy shear zone. Note the phyllonitic amphibolite in the hinge (dark) that acted as a "smear" in the fold hinge between the more competent pegmatite layers. d: Subhorizontally undulating gneissic foliation in the Rong shear zone. e: Asymmetric boudinage of amphibolite layer in gneiss in the Klokkarvik shear zone. f: Asymmetric foliation boudinage in the Toftøy shear zone. g: Train of asymmetric folds (contractional composite structure) in ultramylonite above a biotite-rich décollement in the Skogsøy shear zone. See Fig. 9 for locations. (For interpretation of the references to color in this figure legend, the reader is referred to the Web version of this article.)

4. Shear-zone evolution at different structural levels

To characterize the structural and metamorphic evolution of different levels of the MCC in more detail, we present a description of 23 high-strain zones (Fig. 9) in form of a catalogue (electronic supplement 2) that contains field photos, illustrations and microphotographs. We summarize our observations in Table 1 and classify shear zones with respect to their geometry, lithologies, localization and rheology. In the following, we describe representative shear zones of the different structural levels before we summarize aspects of shear zone evolution during MCC exhumation.

4.1. Bounding shear zones/faults

4.1.1. Austevoll shear zone

The southern bounding shear/fault zone of the ØC is exposed on the island Austevoll, where it merges with the higher-level Sunnhordland detachment (Andersen and Andresen, 1994). The Austevoll locality (Fig. 10) is separated from the ØC by the 700 m-deep Krossfjord. An E-W trending ductile-to-brittle fault zone juxtaposes strongly sheared gneisses with weakly deformed granites of the Sunnhordland batholith (Andersen and Jansen, 1987), which occupied high structural levels of the orogenic wedge (Scheiber et al., 2016). The footwall of the fault consists of a 300 m-wide section of S-dipping mylonitic to ultramylonitic banded gneisses (Fig. 10b) that have characteristics of the Middle Unit with top-to-W and dextral kinematics. Shear fractures host quartz veins and phyllonitic layers show new growth of white mica and chlorite, suggesting the presence of fluids during mylonitization. A zone of granitic and mafic ultramylonites was incised by a steep E-W trending brittle fault zone. In a 10-20 m-wide damage zone the rocks are strongly fractured and shattered, while there is a very discrete fault plane that juxtaposes the embrittled gneisses with fractured granite. Away from the fault, the granite in the hanging wall (Fig. 10c) is weakly deformed except for local shear zones. A large amount of incision and excision

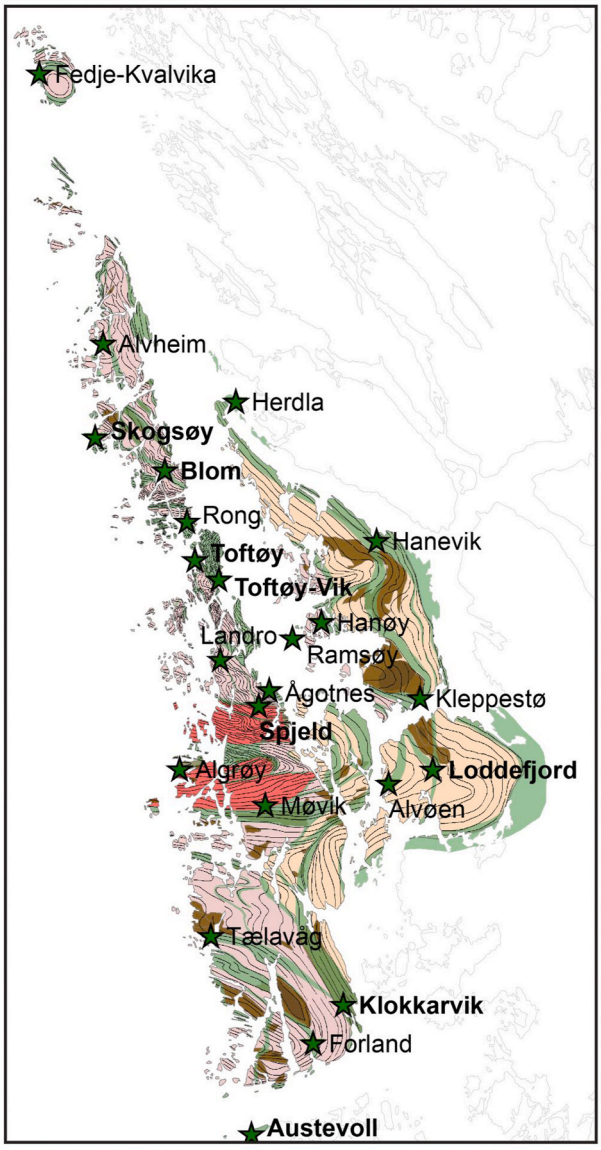

Fig. 9. Map of key shear zones classified in Table 1, illustrated in electronic supplement 2 and described in the text (bold labels).

must have taken place in the fault zone, to juxtapose gneisses from the Middle Unit of the ØC with the upper levels of the Caledonian nappe stack. This fault is cut by coast-parallel faults and fractures that carry Permian dikes (Fossen and Dunlap, 1999), suggesting that it originated prior to North Sea rift initiation. Also, the deep fjord in between the Austevoll locality and the ØC (Fig. 3), invokes the presence of weak rocks (e.g. phyllonites) in a wide shear zone in the footwall of the exposed fault.

4.2. Upper Unit

4.2.1. Loddefjord shear zone

The 300 m-thick, shallowly E-dipping shear zone (Fig. 11a–c) is located structurally ca. 1 km below the eastern boundary of the complex (Wiest et al., 2018b). Anastomosing zones of banded gneisses and mylonitic amphibolites show top-to-E fabrics and contain low-strain lenses of weakly deformed protoliths (Fig. 11a). They show that the Loddefjord shear zone formed in the heterogeneous contact zone between large gabbro and leucogranite bodies (Fig. 11b). Heterogeneous deformation of mafic layers led to boudinage and fracturing of rigid (coarse grained) layers. Abundant veins and hydration of the amphibolites demonstrate fluid ingress along these fractures. Within the alteration zones, biotite replaced amphibole and, if more water was present, biotite was almost entirely replaced by chlorite. Chlorite-phyllonites form layers that are up to 10 m thick and 100s of meters wide. Within these phyllonitic shear zones, the original rheological relationships were reversed. The mafic phyllonites represented the weakest layers and contain fractured and sheared clasts of granitic rocks (Fig. 11c). Small angular granitic clasts were rotated and rounded in the ductile phyllonite matrix (Wiest et al., 2018b, their Fig. 6B), which gave the peculiar-looking fault rock the nickname 'tectonic conglomerate' (Kolderup and Kolderup, 1940). Anastomosing subhorizontal fractures represent the last stage of deformation in the phyllonite shear zones.

4.2.2. Klokkarvik shear zone

This shallowly E-dipping shear zone is up to 800 m-thick and represents the boundary between the Upper and Middle Unit along the eastern coast of Sotra. The Klokkarvik shear zone localized in a highly heterogeneous zone of amphibolites, granitic gneisses and pegmatites (Fig. 11d) that separates relatively weakly deformed homogeneous bodies of granite and gabbro above and below the shear zone, respectively. Fabrics within the shear zone show consistently top-to-ESE kinematics, while top-to-W fabrics are found in the gneisses below (Fig. 6). Lithological heterogeneity and variable deformation of coarse- and fine-grained amphibolites caused large competence contrasts within the shear zone that resulted in ductile-brittle deformation. Boudinage-related fracturing of rigid coarse-grained mafic rocks (Fig. 11d) created pathways for fluids that formed hydrothermal mineralizations of quartz, feldspar and pyrite. Within granitic layers, coarse-grained feldspar-rich pegmatites represent rigid layers and quartz-filled fractures formed at their borders. The quartz veins were themselves mylonitized, while hydration at the contacts formed muscovite (±chlorite) phyllonites (Fig. 11d). These felsic phyllonites show phase-mixing microstructures and the development of micro-shear bands through the connection of muscovite layers (electronic supplement 2).

4.3. Middle Unit

The pervasive deformation in the Middle Unit makes the definitions of shear zones somewhat arbitrary. Yet, some zones show even higher strains than their surroundings and fall into three categories: 1. Strain localization next to weakly deformed bodies, 2. Localization in inherited weak rheologies, 3. Progressive strain-localization during retrograde deformation.

4.3.1. Skogsøy shear zone

Located in the westernmost part of the ØC, where fabrics turn into westward dip, a ca. 50 m-thick subhorizontal shear zone developed at the contact between a leucogranite and Precambrian migmatite (Fig. 12a). The homogeneous leucogranite consists almost entirely of coarse-grained K-feldspar and quartz and contains dismembered mafic boudins. On top of the shear zone, the leucogranite forms a NW-verging fold with NE-plunging fold axes and mineral stretching lineations. Towards the shear zone, grain size decreases continuously, and the mafic bodies become more and more stretched out. The core of the shear zone is a 10 m-thick zone of ultramylonite with shallowly NW-plunging stretching lineations, clear top-to-NW kinematic indicators and sheath folds. The granitic ultramylonite contains rare K-feldspar augen but shows mostly a uniform fine-grained microstructure with evenly distributed feldspar, quartz and finely dispersed biotite. Thin biotite-layers act as small-scale decollements (Fig. 8h).

4.3.2. Blom shear zone

The 200 m-thick shallowly NE-dipping shear zone shows consistent top-to-W kinematics. It represents a heterogeneous zone of mylonitic gneiss, amphibolite, quartzite and sulfidic garnet-micaschist (Fig. 12b).

Table 1
Classification of shear zones illustrated in electronic supplement 2, sorted by units from the highest to the lowest structural level. The first main column shows general features: name, coordinates of the type locality, shear sense, average fabric orientation (dip direction/dip, trend → plunge) and thickness and exposed lateral extent of the shear zone. The second main column (Lithologies) classifies lithologies from high to low metamorphic grade: MI – migmatite, GN – gneiss, AM – amphibolite, QZ – quartzite, MS – micaschist, PH – phyllonite, CA – cataclasite, FG – fault gouge. The third main column (Localization) classifies factors of strain localization: Protolith – localization in weak protolith (e.g. schist), Rim – localization at rim of rigid body, Heterog. – localization in zone of lithological heterogeneity, Boundary – localization at unit boundary. The last main column (Rheology) classifies rheological aspects: Inher. MS – inherited micaschist, Melanos. – inherited biotite melanosomes, Melt – syn-tectonic melt, D-B def. – ductile-brittle deformation, Fluids – Fluid-rock interaction (e.g. veins, hydration reactions, staining), Phyllon. – phyllonitization.

General					Lithologies								Localization				Rheology					
Unit Name	Type locality [°N, °E]	Kinematics	Fabrics Foliation, Lineation	Thickness; Extent	Melt	Ductile						Brittle	Protolith	Rim	Heterog.	Boundary	Melt	Melanos.	Schist	D-B def.	Fluids	Phyllon.
					MI	GN	AM	QZ	MS	PH	CA	FG										
Bounding shear zones/faults																						
Hanevik	60.4992, 5.1532	Top-to-E	050/30, 15->100	1 km; 20 km NW-SE		x	x	x	x	x	x		x		x	x			x	x	x	x
Herdla	60.5787, 4.9696	Top-to-ESE	070/45, 25->110	1 km; 10 km NW-SE		x	x	x	x	x			x		x	x			x	x	x	x
Austevoll	60.1337, 5.0430	Top-to-W; dextral	170/60, 05->270	400 m; 2 km E-W		x	x			x	x				x	x				x	x	x
Upper Unit																						
Klokkarvik	60.2158, 5.1457	Top-to-ESE	060/30, 20->110	800 m; 16 km N-S		x	x			x				x	x	x				x	x	x
Loddefjord	60.3619, 5.2387	Top-to-E	085/20, 10->090	300 m; 8 km N-S		x	x			x	x			x	x					x	x	x
Alvøen	60.3520, 5.1857	Top-to-E	100/15, 15->095	200 m; 4 km N-S		x	x			x				x	x					x	x	x
Kleppestø	60.4049, 5.2179	Top-to-E & -W	040/30, 20->090	<1 km; 11 km N-S		x	x			x	x			x	x	x				x	x	x
Middle Unit																						
Hanøy	60.4479, 5.0913	Top-to-W (& -E)	060/25, 25->090	250 m; 3 km N-S		x	x			x	x				x	x				x	x	x
Ramsøy	60.4367, 5.0568	Top-to-W	030/20, 20->085	200 m; 1 km N-S		x	x	x		x					x					x	x	x
Fedje-Kvalvika	60.7703, 4.6998	Top-to-NW	315/35, 40->310	600 m; around dome		x		x	x	x			x		x			x	x	x	x	x
Alvheim	60.6088, 4.8009	Top-to-W	070/05, 03->100	100 m; 4 km N-S		x		x	x				x		x			x	x	x	x	
Skogsøy	60.5515, 4.7986	Top-to-NW	310/05, 02->310	50 m; 1 km N-S		x	x			x				x	x			x		x	x	x
Blom	60.5342, 4.8867	Top-to-W	050/25, 10->100	200 m; 4 km NW-SE		x	x	x	x	x		x	x		x			x	x	x	x	x
Rong	60.4943, 4.9196	Top-to-W	035/20, 05->280	350 m; 3 km E-W		x	x	x		x					x			x		x	x	x
Toftøy	60.4807, 4.9308	Top-to-W	065/20, 15->100	800 m; 5 km N-S		x	x	x	x	x			x		x			x	x	x	x	x
Toftøy-Vik	60.4698, 4.9616	Top-to-WNW	070/15, 10->110	50 m; 3 km N-S		x	x	x		x					x					x	x	x
Tælavåg	60.2525, 4.9787	Top-to-WNW	020/25, 15->110	300 m; 10 km NW-SE		x	x			x				x	x					x	x	x
Forland	60.1914, 5.1117	Top-to-W	060/20, 05->100	150 m; 5 km N-S		x	x			x				x	x					x	x	x
Landro	60.4211, 4.9697	Top-to-W	020/25, 15->090	100 m; 3 km NW-SE	x	x	x			x		x			x	x	x	x		x	x	x
Ågotnes	60.4045, 5.0321	Coaxial; Top-to-W (& -E)	060/30, 15->080	200 m; 4 km N-S	x	x	x			x	x	x			x	x	x	x		x	x	x
Lower Unit																						
Algrøy	60.3531, 4.9281	Top-to-W	160/40, 05->085	500 m; 2 km E-W	x	x	x			x					x	x	x	x		x	x	x
Møvik	60.3343, 5.0357	Sinistral	175/50, 10->090	1 km; 10 km E-W	x	x	x		x	x	x		x		x	x	x	x	x	x	x	x
Spjeld	60.3946, 5.0204	Coaxial, sinistral	000/80, 05->095	200 m; 5 km E-W	x	x	x			x					x	x	x	x		x	x	x

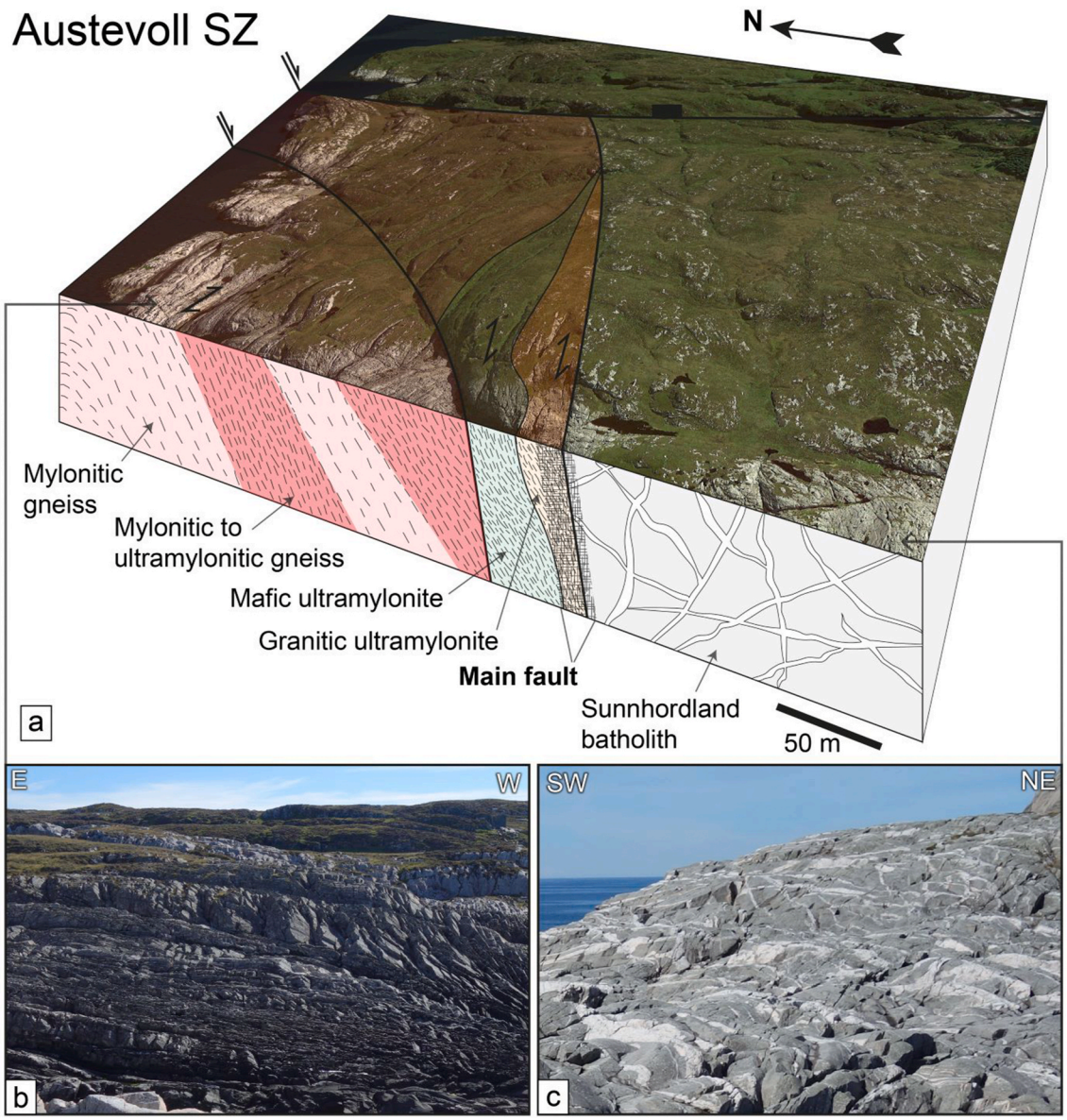

Fig. 10. The Austevoll locality exposes the southern bounding shear zone/fault of the ØC. The main fault juxtaposes strongly sheared gneisses from the ØC (b, width of view ca. 100 m) with weakly deformed granite of the Upper Allochthon Sunnhordland batholith (c, width of view ca. 150 m). Image from Google Earth.

The protolith relationships suggest that the quartzite/schist lenses are resisters, which escaped Precambrian migmatization, and represent inherited weak layers that localized Caledonian shearing. In the largest, ca. 5–10 m thick schist layer folded and mylonitized quartz veins are abundant. These brittle-ductile fabrics are cut by a foliation-parallel, dm-thick subhorizontal fault gouge (Fig. 12b), which in turn is cut by steep brittle faults and fractures of Early Devonian age (Larsen et al., 2003).

4.3.3. Toftøy shear zone

The Toftøy shear zone (Fig. 12c) represents a wide zone of strongly deformed gneisses that locally contain weakly deformed Precambrian migmatites. Foliations dip shallowly to the east and are folded along lineation-parallel ESE-plunging recumbent folds (Fig. 8c). Kinematic indicators show consistently top-to-W kinematics. Abundant biotite-décollements controlled the evolution of shear zone structures in the gneisses (Fossen and Rykkelid, 1990, 1992; Rykkelid and Fossen, 1992). These biotite layers formed either as melanosomes of Precambrian stromatic metatexites (cm-thick, several m^2 lateral extent) or as retrogressed amphibolite layers (m-thick, several km^2 lateral extent). The metatexites are more strongly deformed than neighboring quartzitic gneisses. Vertical shortening through recumbent folding allowed the formation of laterally extensive, subhorizontal high-strain zones that show progressive strain-localization during retrograde deformation and hydration of mafic layers. The best exposures of these processes are found in the Toftøy-Vik locality, which is part of a 3 km-long, shallowly E-dipping ductile-to-brittle fault zone (Fig. 12c–e). Amphibolite-facies gneisses show boudinage of mafic layers, while some large amphibolite layers are transformed into chlorite-biotite phyllonite (Fig. 12d) and form a 'tectonic conglomerate' with fractured granitic clasts in a sheared phyllonite matrix (Fig. 12d and e). Compared to the phyllonite zones in the Upper Unit, however, these phyllonites are coarser grained and show top-to-W kinematics.

4.4. Lower Unit

4.4.1. Spjeld shear zone

The steeply N-dipping Spjeld shear zone represents the northern

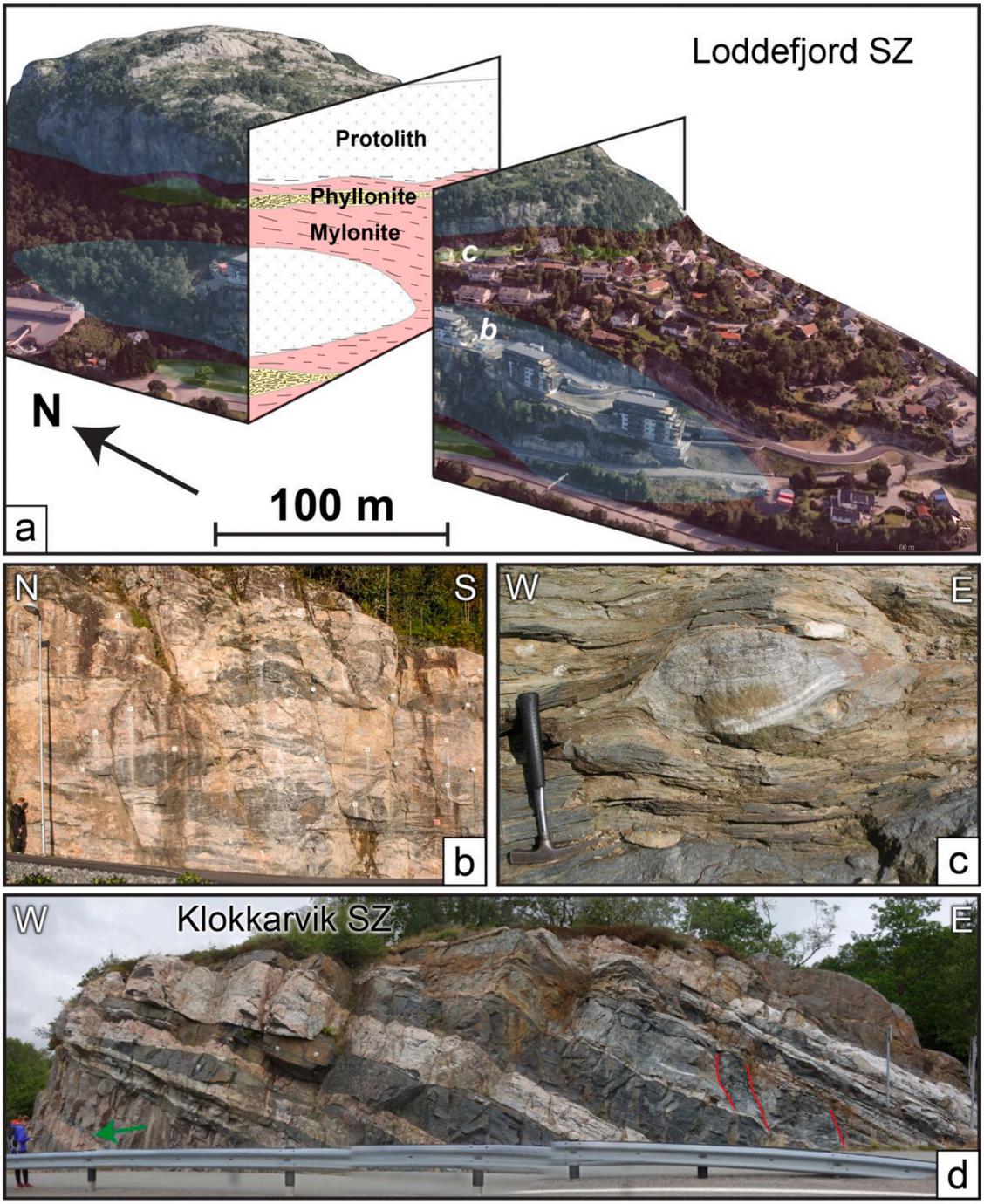

Fig. 11. Shear zones in the Upper Unit. a: Architecture of the Loddefjord shear zone based on a surface model from Google Earth that is cut open in E-W direction. The location of b and c is marked in the image. b: Low strain lens revealing the heterogeneity of the protolith: A Sveconorwegian intrusive complex consisting of granites (orange-pink) and mafic lenses. Person for scale. c: Sheared clast of granitic gneiss contained within chlorite phyllonite that formed from amphibolite. The clast has a mixed δ- and σ-shape and indicates top-to-E shear sense. Hammer for scale. d: Panoramic photo stitch showing a heterogeneous low-strain domain of the Klokkarvik shear zone with granitic gneiss, pegmatite and amphibolite. Asymmetric shear fractures (red lines) are developed in a coarse-grained amphibolite layer, while fine-grained amphibolites (black) deform ductilely. Compositional variations in the granitic gneiss lead to fracturing, fluid ingress and phyllonitization (green arrow). Person for scale. (For interpretation of the references to color in this figure legend, the reader is referred to the Web version of this article.)

boundary of the migmatite domain. The migmatites in this zone contain a tract of highly reactive garnet-staurolite amphibolites with three distinct fabric domains that record a progressive evolution from high to low grade (Fig. 13). Domain 1 consists of meter-scale lenses of unfoliated amphibolite, which contains no macroscopically visible plagioclase. The rock consists of large, unoriented amphiboles and garnet and skeletal staurolite crystals reaching up to 10 cm in diameter. Rutile inclusions occur commonly in garnet and Johns (1981) describes occurrences of kyanite. The rock contains veins consisting entirely of garnet and plagioclase-garnet-staurolite leucosomes at the boundary to Domain 2. The latter consists of coarse-grained amphibolites that contain abundant plagioclase and have a well-developed vertical foliation that wraps around the Domain 1 lenses. Plagioclase shows textures indicative of partial melting and occurs commonly around garnet that is replaced by

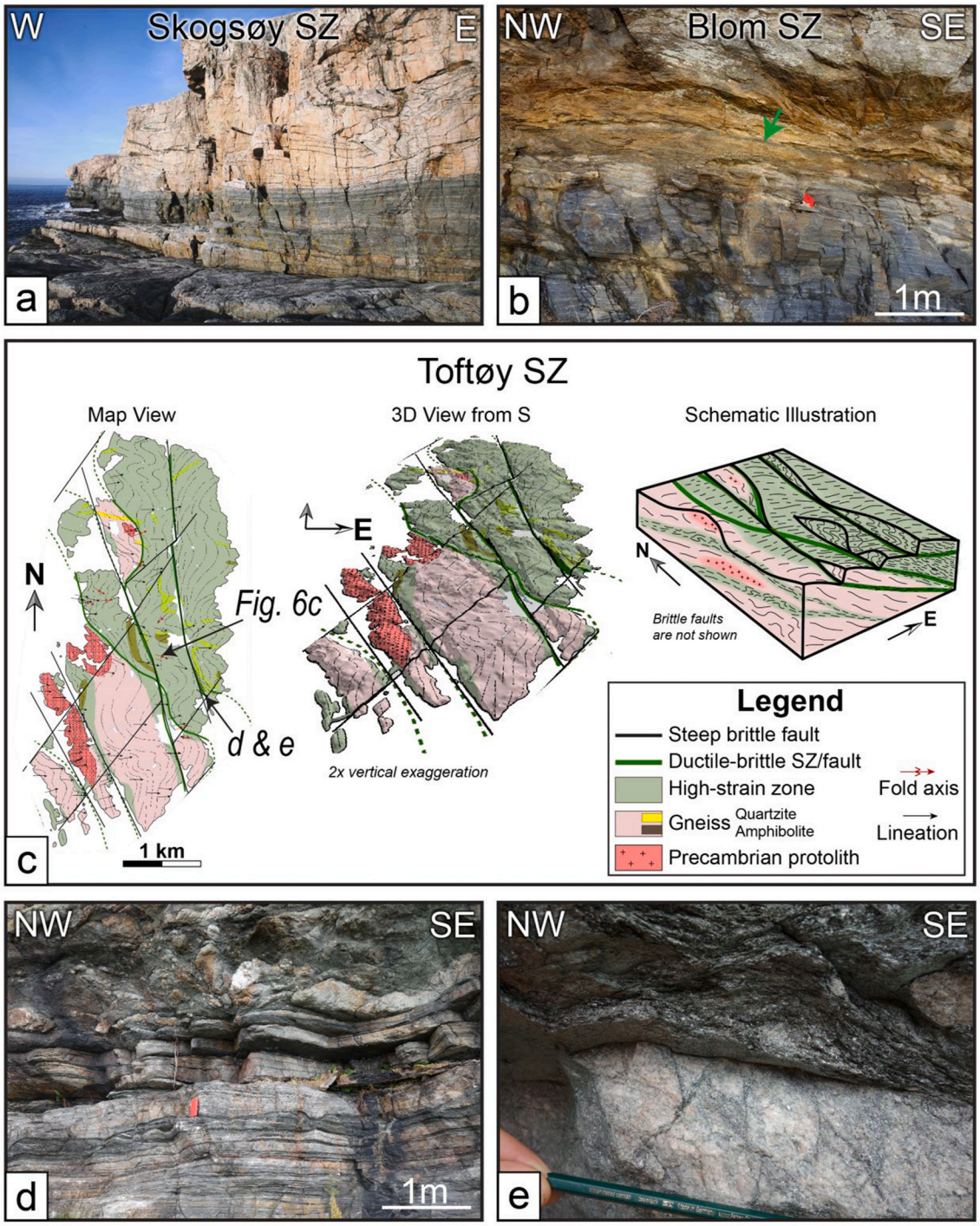

Fig. 12. Shear zones in the Middle Unit. A: The Skogsøy shear zone developed at the base of a homogeneous orange leucogranite. The granite contains mafic bodies that become more and more stretched out towards the shear zone. The dark color of the shear zone is the result of extreme grain-size reduction in the ultramylonite. Note person for scale. B: Blom shear zone. A subhorizontal fault gouge (red arrow) cuts through a layer of garnet-micaschist that is surrounded by gneiss. C: Architecture of the Toftøy shear zone. D: The Toftøy-Vik shear zone consists of a wide zone of mylonites that developed into a localized ductile-brittle shear zone. The lower part of the outcrop shows a mylonitic gneiss with a boudinaged amphibolite layer. The upper part of the outcrop consists of a larger amphibolite layer that has been hydrated into a chlorite-biotite phyllonite that contains granitic clasts. E: Detail from the "tectonic conglomerate" showing small-scale chlorite-filled fractures in a large granitic clast contained in phyllonite. Note rounded clast on the upper right side. (For interpretation of the references to color in this figure legend, the reader is referred to the Web version of this article.)

magnetite. Solid-state symmetric fabrics show coaxial stretching in E-W direction, but asymmetric foliation boudinage indicates a sinistral sense of shear. Domain 3 is a coarse-grained chlorite phyllonite shear zone cutting obliquely through the Domain 2 fabric. The shear zone developed along a vertical fracture with thick plagioclase-quartz veins that served as a pathway for fluids, which hydrated the rock so that all mafic phases were replaced by chlorite.

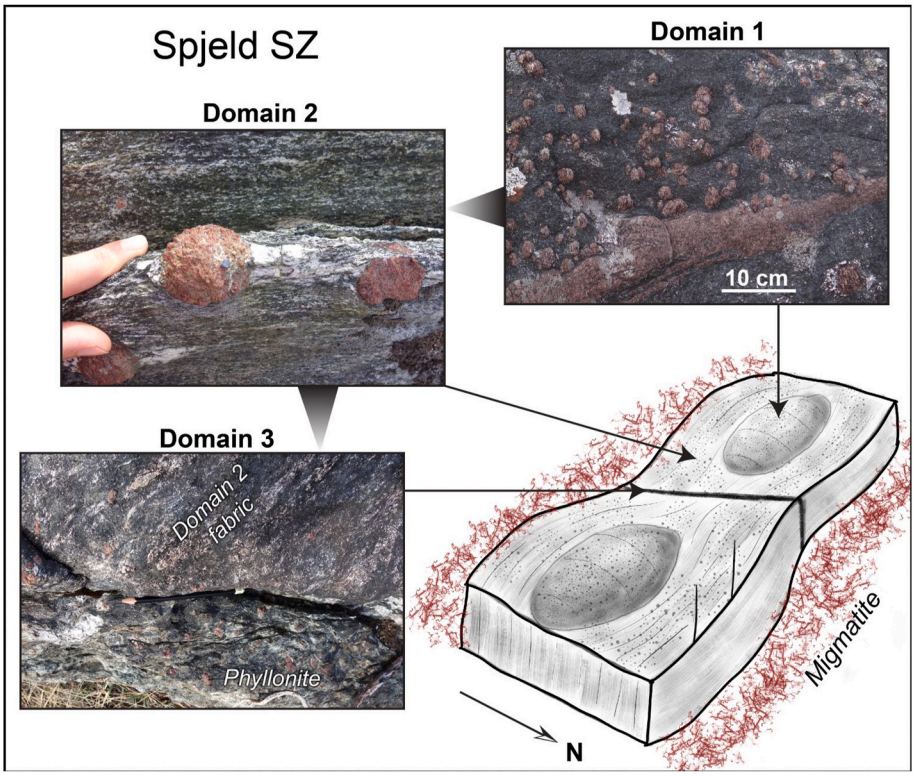

Fig. 13. Migmatites in the Spjeld shear zone contain a suite of garnet-staurolite amphibolite xenoliths that record a progressive evolution in three distinct domains. Domain 1: Unfoliated ultramafic amphibolite (no plagioclase) with large garnets and staurolites and garnet veins. Domain 2: Foliated amphibolite with plagioclase and large garnet pophyroclasts with symmetric plagioclase strain fringes. Domain 3: Chlorite-phyllonite shear zone cutting through Domain 2 fabric along a brittle fracture (pencil for scale).

4.5. Shear zones and structures across the scales

Some of the described structures and processes are self-similar on different scales, while others are not (Fig. 14). Necking occurs from the microscale, affecting minerals, to the crustal-scale forming an entire MCC. Folds are recumbent on the mesoscale, but upright on the macro- and megascale. Coherent migmatite bodies are observed up to the km-scale, however, the extent of migmatites at deeper levels of the complex could be larger. The mapped migmatites coincide precisely with an E-W-elongated positive magnetic anomaly (Gellein, 2007a). Similar anomalies in other parts of the complex might indicate unexposed migmatite bodies that could be connected at depth as indicated in Fig. 4.

Based on Table 1 we can assess micro-to mesoscale aspects of shear zone localization and rheology. Shear zones localized either in inherited weak zones, at the rim of weakly deformed rigid bodies or at unit boundaries and always represent zones of strong lithological heterogeneity. Phyllosilicates, either inherited or newly formed, played an important role in many shear zones. Phyllosilicate layers were inherited in form of melanosomes in stromatic metatexites or schist layers that escaped migmatization. Lithological heterogeneity and variable shearing of coarse-grained (rigid) and fine-grained layers lead to brittle-ductile deformation. Fluid ingress along shear fractures was associated with retrograde hydration, especially of mafic rocks. Biotite-phyllonites formed from retrogressed amphibolites are very common, but usually no more than a few decimeters thick. Individual bodies of chlorite (±biotite)-phyllonites, which formed through advanced hydration of mafic layers, can be up to 10 m thick, but shear zones commonly contain multiple levels of phyllonites. Muscovite-quartz phyllonites formed through hydration of felspar-rich granitic rocks but are less common.

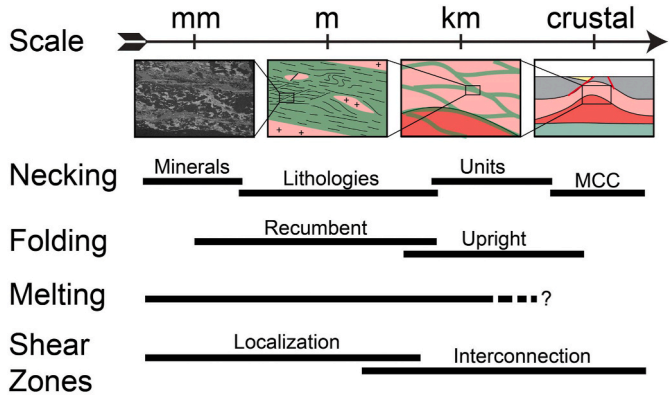

Fig. 14. Schematic illustration of different structures and processes and the scales they occur on. Necking can be observed to affect different entities in a self-similar manner. The fold style, on the other hand, shows scale-dependent variations. The same accounts for the observed extent of partial melting and solid-state shear zones. Different processes control shear-zone localization, but in order to control the crustal-scale rheology, they must form an interconnected network.

When trying to extrapolate our outcrop-scale observations, it becomes clear that the inherited as well as newly formed weak décollements could have controlled the rheology of the ductile crust, as soon as they formed an interconnected shear zone network. The map-scale pattern of shear zones suggests this as a plausible scenario in the case of the ØC. Inside these shear zones, however, a multitude of factors and processes determined the rheology, which furthermore evolved over time. During retrogression, ductile-to-brittle deformation became progressively localized into weak phyllosilicate horizons until the last increment represented by subhorizontal, foliation-parallel fault gouges that are cut by Early Devonian steep faults (Larsen et al., 2003).

5. Discussion

5.1. The Øygarden Complex – A bivergent MCC

We have shown that the ØC is a ductile dome that contains structures formed at different crustal levels. Retrogressive E-W stretching with increasing strain intensity from top to bottom formed ductile-to-brittle

shear zones at all exposed structural levels. This deformation includes simple shear, vertical shortening and low-grade retrogression, which is characteristic for the footwall of continental detachment systems (Whitney et al., 2013). Available dates from the ØC show an evolution from partial melt crystallization (U–Pb zircon leucosomes: ~405 Ma) to rapid exhumation of ductile crust (Ar–Ar white mica and biotite: mostly 405–399 Ma) (Boundy et al., 1996; Fossen and Dunlap, 1998; Wiest, 2020) reaching brittle conditions around ca. 396 Ma (Fossen et al., 2016; Larsen et al., 2003). These ages correspond to post-orogenic collapse in a regime of sinistral transtension (Fossen, 2000; Fossen et al., 2013; Krabbendam and Dewey, 1998; Osmundsen and Andersen, 2001). Today, the ØC is in contact with remnants of Devonian supradetachment basins (north), uppermost parts of the orogenic wedge (south) and various nappes of the Bergen Arc system (Fig. 3). As discussed by Wiest et al. (2018b), the eastern contact of the ØC can be considered as an E-directed detachment that reactivated the original basal thrust (Fossen, 1989) with variable amounts of excision. Besides, parallel reflectors in near-shore seismic data suggest a shallowly W-dipping detachment offshore (Fossen et al., 2016). This is also indicated by the westward rotation of fabrics into westerly dip associated with dominant top-to-W kinematics, top-to-W shear zones at the southern and northern tips of the complex, and overlaying Devonian supradetachment basins. Although not exposed, the location of this western detachment can be inferred from a pronounced E-W-trending magnetic anomaly (Gellein, 2007a) that corresponds precisely to the mapped migmatite domain. All of the aforementioned points suggest that the ØC represents a bivergent MCC, exhumed during post-orogenic collapse.

5.2. Boundary conditions of post-orogenic MCC formation

A post-orogenic MCC model agrees with the boundary conditions of the Bergen Arc system. Although ductile flow might have occurred during convergence (see section 5.3), we found no structures in the ØC that can be clearly assigned to this stage. In the overlaying nappes of the Bergen Arcs system, in contrast, ages and structures related to syn-convergent deformation and exhumation are abundant (Fossen, 1988, 1989; Fossen and Dunlap, 1998, 2006; Jolivet et al., 2005; Kuhn et al., 2002). This conforms with the notion, that the Baltican margin was cool and rigid during continental subduction so that deformation became localized into the overlaying basal décollement and weak allochthons (Butler et al., 2015; Fauconnier et al., 2014; Fossen, 1992). Post-orogenic extension, on the other hand, affected an overthickened and thermally softened, but rheologically highly heterogeneous crust. The orogenic wedge was relatively cold and consisted of various thrust nappes with very distinct histories and rheologies (Fossen et al., 2017). The Bergen Arcs system is mostly occupied by dry lower-crustal rocks of the Lindås Nappe (Austrheim, 2013) and the Gullfjellet Ophiolite, which represented both rigid and dense bodies (Gellein, 2007b). Structurally underneath, the km-thick thrust-related mylonites and schists of the Minor and Major Bergen Arcs (Faerseth et al., 2011; Fossen, 1989) constituted décollements localizing deformation. The three map units within the ØC and their structural characteristics can be interpreted as rheological layers with downward decreasing viscosity. The boundary between the Upper and Middle Unit represents the transition from localized to distributed strain (Cooper et al., 2017), while the limit of partial melting defines the Lower Unit. Highly radioactive granites (Pascal and Rudlang, 2016) may have caused a thermal anomaly in the ØC. Previously, late Caledonian partial melting has been reported only

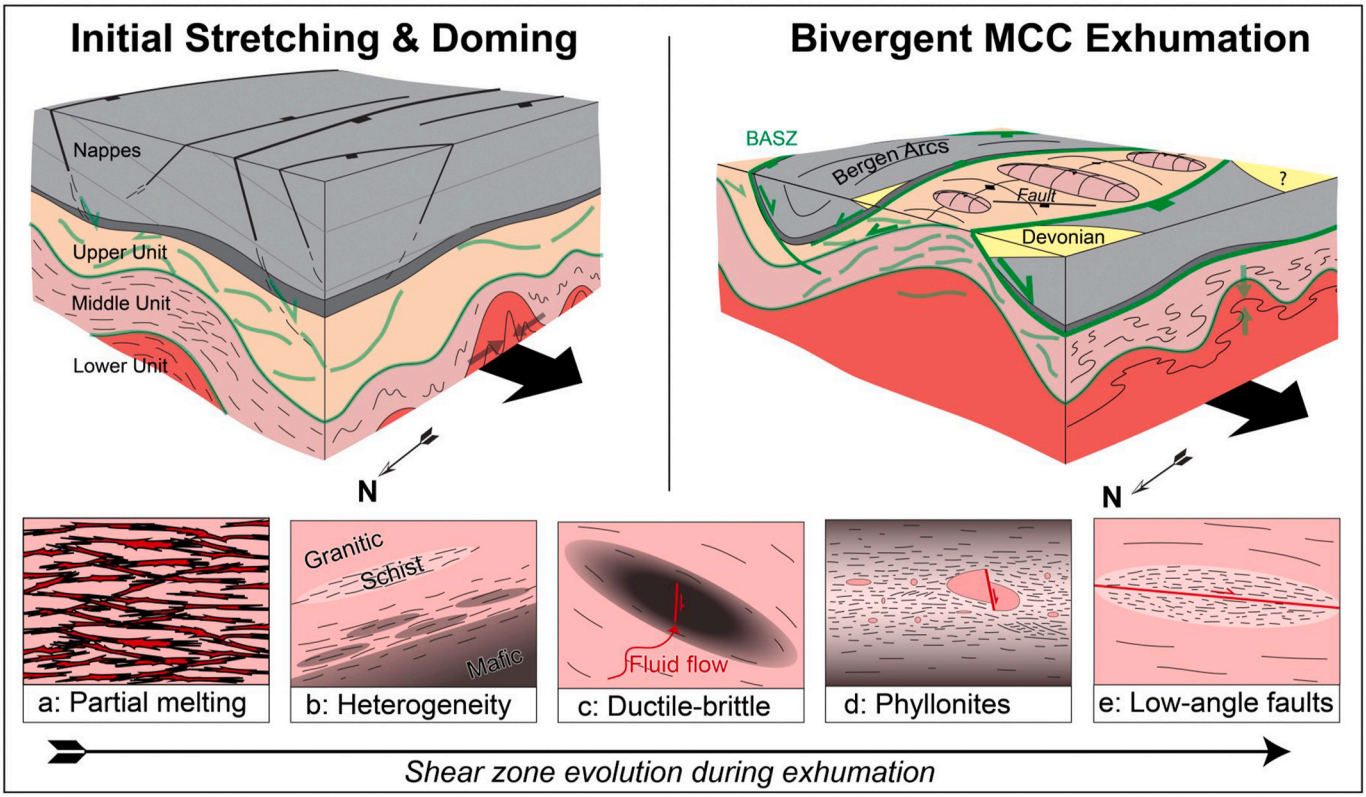

Fig. 15. Schematic illustration of the proposed MCC model for the ØC. Initial stretching of the rheologically layered orogenic crust caused ductile necking, doming and extension-perpendicular shortening in the deep crust. Strain-weakening feedbacks, illustrated in panels (a–e), led to retrogressive overprinting, vertical shortening and the formation of interconnected weak décollements (green). The shear zone evolution contributed to the formation of bivergent detachments, which eventually exhumed the MCC, while dense nappes in the Bergen Arcs sank into a 'ductile graben' structure. Note, we do not imply that the ØC was exhumed to the surface. (For interpretation of the references to color in this figure legend, the reader is referred to the Web version of this article.)

from the highest-grade regions of the Western Gneiss Region (Gordon et al., 2013, 2016; Hacker et al., 2010; Kylander-Clark and Hacker, 2014; Labrousse et al., 2004, 2011). The rheological layering, inferred for the Bergen Arcs system and the underlying ØC (Fig. 15) at the onset of post-orogenic extension, represents a first-order parameter controlling intra-crustal necking and MCC formation (Huet et al., 2011; Labrousse et al., 2016; Wijns et al., 2005).

5.3. Formation of the Øygarden dome and the Bergen Arcs

The formation of domes is commonly controversial (Yin, 2004) and the ØC is no exception. The juxtaposition of the migmatite domain with strongly deformed, but solid-state structural levels suggests that the Øygarden dome formed within the ductile (plastic) crust. This could have happened during convergence or initial post-orogenic extension. The peculiar relation of opposing shear senses at upper and lower levels of the ØC inevitably invokes comparison with models of channel flow (Grujic, 2006) or 'compressional MCCs' (Searle and Lamont, 2020). Doming and top-to-W fabrics above the migmatite domain could be related to horizontal eastward flow of a partially molten layer during ongoing convergence ('channel detachment' by Teyssier et al., 2005). Such a model, however, does not explain the systematic retrogressive overprinting of fabrics with consistent, but opposing kinematics in different domains. Alternatively, the opposing shear senses might represent westward extrusion of a ductile nappe similar to the Greater Himalayan Series (Grujic et al., 1996). However, this model is not supported by the regional structural context (Fossen, 2000; Fossen et al., 2014) and available geochronological data (Wiest, 2020). A more consistent explanation may be provided by transtensional doming during post-orogenic collapse involving westward ductile extrusion of high-grade, low-viscosity material at lower levels.

In the latter scenario (Fig. 15), initial stretching of the rheologically layered orogenic crust caused upper crustal faulting, while necking instabilities developed in the ductile crust. The inverted rheological and density structure with the Lindås Nappe and Gullfjellet Ophiolite on top of partially molten granitic basement induced doming of the ØC. Inside the basement, necking of upper levels was compensated by extension-perpendicular shortening within the lower levels, forming mega-scale upright folds including the migmatite double-dome (Le Pourhiet et al., 2012; Rey et al., 2017; Wiest et al., 2019). During continued crustal stretching, these structures were progressively overprinted by bivergent detachments. As a result, the dense nappes sank into an arcuate synformal structure, caught in between the concave Bergen Arcs Shear Zone (Wennberg et al., 1998) and the convex eastern detachment wrapping around the Øygarden dome (Fig. 15). Considering the deep erosion level, the structural relationship of the ØC and Bergen Arcs can thus be seen as ductile equivalents to horsts and grabens.

5.4. Shear zone evolution during MCC exhumation

Indifferent of these models, we can discuss factors that controlled the rheology within the exhuming shear zones. The observed amount of leucosomes in the Lower Unit of the ØC (Fig. 15a) suggests that the presence of melt initially controlled deep crustal flow (Rosenberg and Handy, 2005), while high temperatures activated pervasive ductile flow in the Middle Unit. In the Upper Unit, preexisting lithological heterogeneity (Fig. 15b) appears as the main parameter that controlled shear zone localization (Pennacchioni and Mancktelow, 2007) and became progressively more important for the lower levels. Competence contrasts related to variable mineralogy and grain size led to ductile-brittle deformation and channelized fluid flow in shear fractures (Fig. 15c). The ØC shows evidence of abundant syn-tectonic fluids of probable metamorphic and/or magmatic origin (Quilichini et al., 2016; Siebenaller et al., 2012; Whitney et al., 2013). There must have been significant permeability in the ductile crust, to allow the large fluid fluxes that are needed to form the observed chlorite phyllonites (Fig. 15d). Chlorite contains on average 5 times as much water as amphiboles and 3 times as much as mica (Hacker et al., 2003a). If we consider for example an ellipsoid-shaped amphibolite body with dimensions 100 m × 150 m x 10 m (corresponding to one of the larger phyllonite bodies observed in the Loddefjord shear zone) that consisted of 50% amphibole, an influx of roughly 2 million liters of water would be needed to convert all the amphibole to chlorite. Fluids could have moved through shear zones by intergranular processes, such as creep cavitation (Fusseis et al., 2009), yet, on the mesoscale we observe ductile-brittle fracturing (Fig. 15c) as the major mechanism providing transient permeability. The relative abundance of pervasively phyllonitized amphibolites compared to granitic rocks implies a higher reactive potential for fluid-rock interaction in mafic rocks (Kleine et al., 2015). Furthermore, the fabric weakening associated with fluid-induced retrogressive phyllosilicate growth (Bos and Spiers, 2002) activated a feedback loop of shearing, channelized fluid flow and phyllonitization. This made mafic rocks sinks for fluids and turned them into the weakest layers, in stark contrast to their expected behavior at low metamorphic grades. During exhumation and retrogression, deformation progressively localized into phyllosilicate-rich décollements, either inherited (melanosomes and schists) or newly formed (phyllonites), eventually forming sub-horizontal brittle faults (Fig. 15e). If we assume that these décollements were interconnected in a self-similar manner across the scales (Fig. 14), the rheology of phyllosilicates (Aslin et al., 2019; Bos and Spiers, 2002; Hunter et al., 2016; Wintsch et al., 1995) controlled the deformation of the exhuming ductile crust at some stage.

5.5. Comparison with other MCCs

Considering the rheological profile of the crust, the ØC appears to represent an intermediate case in between classical "Cordilleran metamorphic core complexes" without migmatization (e.g. Armstrong, 1982; Coney, 1980; Platt et al., 2015) and migmatite-cored MCCs hosting gneiss domes with extensive melting such as the Cordilleran Shuswap MCC (Norlander et al., 2002; Teyssier et al., 2005; Vanderhaeghe et al., 1999, 2003), the Aegean Naxos MCC (Cao et al., 2013; Jolivet et al., 2004; Vanderhaeghe et al., 2004) or the Variscan Montaigne Noire dome (Brun and Van den Driessche, 1994; Roger et al., 2015; Whitney et al., 2015). Besides the geological setting of orogenic collapse, the ØC resembles these MCCs also in other aspects. Despite the difference in erosion level, the similarity between Caledonian and Cordilleran MCCs has long been noted (McClay et al., 1986). The ØC shows similar Precambrian basement rocks in the core, opposed shear senses (Cooper et al., 2010) and a downward succession from localized to distributed (solid-state) deformation (Cooper et al., 2017). The inferred structure of the migmatite double-dome, on the other hand, resembles the Montagne Noire and Naxos MCCs (Kruckenberg et al., 2011; Rey et al., 2017; Roger et al., 2015). The exotic garnet-staurolite amphibolites described in Section 4.4 might indicate that the ØC migmatites sampled portions of the lower crust and transported them upwards in a manner similar to the model proposed by Whitney et al. (2015) for the Montagne Noir eclogites. Rutile inclusions in garnets suggest that these amphibolites experienced pressures above 10 kbar (Zack and Kooijman, 2017), assuming that the rutile is metamorphic, which is 2 kbar higher than the only previously published thermobarometric estimate from the ØC (Boundy et al., 1996). Low-grade retrogression involving fluid alteration, has affected all structural levels of the Naxos MCC (Cao et al., 2017). The retrogressive shear zone evolution described in this study can be better understood by comparing the ØC to nearby MCCs in W Norway.

Coaxial stretching and deep crustal necking, followed by detachment-related simple shearing, is characteristic for most of the Western Gneiss Region and the extensional system of SW Norway (Andersen and Jamtveit, 1990; Andersen et al., 1994; Fossen, 2010; Hacker et al., 2010; Labrousse et al., 2002, 2004; Wiest et al., 2019). Although an order of magnitude smaller, the ØC structurally resembles

the Central Norway basement window (Braathen et al., 2000). More directly, it can be compared with the neighboring Gulen MCC (Fig. 2). While syn-extensional melting was absent at the exposed level of the Gulen dome (Wiest et al., 2019), deep crustal extension-perpendicular inward flow of solid-state low-viscosity material formed a high-grade core with abundant eclogites, coaxial strain, subvertical foliations and isoclinal upright folds parallel to subhorizontal lineations. Wrapping around the core, detachment mylonites are distinguished by retrograde simple shear deformation, vertical shortening and low-grade retrograde deformation involving fluid-rock interaction. Why was a high-grade core preserved in the Gulen MCC, while the entire ØC shows characteristics of detachment shearing? The Gulen MCC apparently experienced higher pressures during continental subduction, although retrogression may just have obliterated any traces of eclogite-facies metamorphism in the ØC (note the description of rutile inclusions in garnet in section 4.4). On the other hand, the crust in the ØC had either a higher geothermal gradient because of especially heat-producing granites (Pascal and Rudlang, 2016) or experienced higher strain rates, so that migmatites were exhumed from a deeper crustal level (Rey et al., 2009). Most importantly, however, fluids seem to have been more abundant in the ØC and triggered a weakening feedback in the exhuming ductile crust. The exact source of these fluids is yet unknown, but we note the location of the ØC above a postulated extinct Sveconorwegian mantle wedge, which might have been hotter and more hydrous than average lithospheric mantle (Slagstad et al., 2018a). Lastly, the ØC is the only MCC exposed in the hanging wall of the main detachment system that runs along the west coast of southern Norway (Fig. 2). An important implication of this point is the possible existence of multiple levels of (bivergent) detachments and MCCs in the North Sea region, which could have influenced rifting (Fazlikhani et al., 2017).

5.6. *Comparison with models and implication for detachments*

Based on numerical and analogue models (e.g. Brun et al., 1994; Tirel et al., 2008; Tirel et al., 2006), Brun et al. (2018) suggest that detachments must not necessarily initiate at the onset of extension, but can evolve progressively during exhumation of ductile crust. This model-based idea conforms very well with our observations from the ØC. We see a km-wide 'processing zone' in the ductile crust where retrogressive shearing forms an interconnected network of inherited and newly formed phyllosilicate-rich décollements (Fig. 16). The ØC might represent an extreme end-member case, caused by the excessive abundance of fluids. Still, similar processes could be essential for detachments in general, given their consistent ductile-to-brittle evolution and the important role of phyllosilicates within such structures (Bos and Spiers, 2002; Collettini et al., 2009a; Hunter et al., 2016; Whitney et al., 2013; Wintsch et al., 1995).

This idea could help to resolve an apparent paradox in the formation of extensional continental detachments. A high intra-crustal strength contrast is needed for internal necking of the crust (Labrousse et al., 2016), as opposed to wide rifting or whole-crust necking compensated by mantle flow (Brun et al., 2018; Buck, 1991). On the other hand, the thickness (and hence the strength) of the brittle layer limits localization on a single detachment fault (Lavier and Buck, 2002; Lavier et al., 1999). So, while a strong brittle layer is mandatory for intra-crustal necking, it impedes the formation of MCCs. Based on our model of the ØC, we speculate that retrogressive shearing triggers positive weakening feedbacks, which reduce the viscous strength of the exhuming ductile crust. This effectively reduces also the thickness of the brittle layer, allowing brittle deformation to localize into single faults that eventually become detachments.

6. Conclusions

We explain the structure of the ØC and the Bergen Arcs by bivergent MCC exhumation during post-orogenic collapse. Extension of a rheologically layered orogenic crust led to necking and doming controlled by viscous flow of the (partially molten) Baltic Shield basement. Lithological heterogeneity during shearing triggered a feedback loop of ductile-brittle deformation, channelized fluid flow and retrogressive

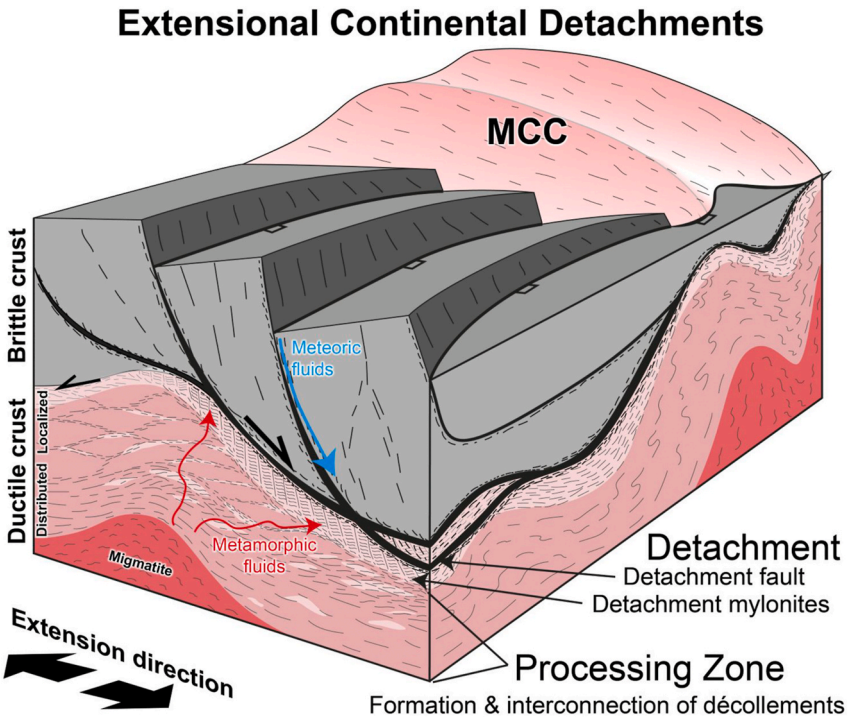

Fig. 16. Suggested model of extensional continental detachments based on the ØC. In a km-wide processing zone, the formation and interconnection of décollements (light shade) weakens the ductile crust. The accumulation of these weak, phyllosilicate-rich layers forms detachment mylonites and promotes slip of low-angle brittle faults. (For interpretation of the references to color in this figure legend, the reader is referred to the Web version of this article.)

phyllosilicate growth, which caused fabric weakening particularly in mafic layers. The interconnection of inherited and newly-formed, phyllosilicate-rich décollements controlled the progressive localization of deformation. The associated weakening of the exhuming ductile crust promoted the formation of bivergent detachments that juxtaposed the Øygarden dome with Devonian supradetachment basins and high levels of the former orogenic wedge. Our results suggest that retrogressive weakening can occur in a kilometer-wide ductile-to-brittle 'processing zone' and represents an essential mechanism for the progressive formation of continental detachments.

CRediT authorship contribution statement

J.D. Wiest: Conceptualization, Formal analysis, Investigation, Writing - original draft, Visualization, Funding acquisition. **H. Fossen:** Conceptualization, Investigation, Writing - review & editing, Supervision, Funding acquisition. **J. Jacobs:** Conceptualization, Writing - review & editing, Supervision, Project administration, Funding acquisition.

Declaration of competing interest

The authors declare that they have no known competing financial interests or personal relationships that could have appeared to influence the work reported in this paper.

Acknowledgements

We are grateful for constructive reviews by Whitney Behr and Olivier Vanderhaeghe and editorial handling by Stephen Laubach. We thank Irina Dumitru and Irene Heggstad at UiB for help with sample preparation and BSE imaging. JDW thanks everyone who joined in the field and in particular Thilo Wrona, Eric Salomon and Sebastian Wolf. This work was funded by VISTA [grant number 6271] – a basic research program in collaboration between the Norwegian Academy of Science and Letters, and Equinor.

Appendix A. Supplementary data

Supplementary data to this article can be found online at https://doi.org/10.1016/j.jsg.2020.104139.

References

Andersen, T.B., Andresen, A., 1994. Stratigraphy, tectonostratigraphy and the accretion of outboard terranes in the Caledonides of Sunnhordland, W. Norway. Tectonophysics 231, 71–84.
Andersen, T.B., Bering, D.H., Fossen, H., Ingdahl, S.E., Jansen, Ø.D., Rykkelid, E., Thon, A., 1988. Berggrunnskart Austevoll 1115-2 M 1:50.000. Norges geologiske undersøkelse.
Andersen, T.B., Corfu, F., Labrousse, L., Osmundsen, P.T., 2012. Evidence for hyperextension along the pre-Caledonian margin of Baltica. J. Geol. Soc. 169, 601–612.
Andersen, T.B., Jamtveit, B., 1990. Uplift of deep crust during orogenic extensional collapse - a model based on field studies in the sogn-sunnfjord region of western Norway. Tectonics 9, 1097–1111.
Andersen, T.B., Jamtveit, B., Dewey, J.F., Swensson, E., 1991. Subduction and eduction of continental-crust - major mechanisms during continent-continent collision and orogenic extensional collapse, a model based on the south Norwegian Caledonides. Terra. Nova 3, 303–310.
Andersen, T.B., Jansen, O.J., 1987. The Sunnhordland batholith, W Norway - regional setting and internal structure, with emphasis on the granitoid plutons. Nor. Geol. Tidsskr. 67, 159–183.
Andersen, T.B., Osmundsen, P.T., Jolivet, L., 1994. Deep crustal fabrics and a model for the extensional collapse of the southwest Norwegian Caledonides. J. Struct. Geol. 16, 1191–1203.
Andresen, A., Rehnström, E.F., Holte, M., 2007. Evidence for simultaneous contraction and extension at different crustal levels during the Caledonian orogeny in NE Greenland. J. Geol. Soc. 164, 869–880.
Armstrong, R.L., 1972. Low-angle (denudation) faults, hinterland of sevier orogenic belt, eastern Nevada and western Utah. Geol. Soc. Am. Bull. 83, 1729–1754.
Armstrong, R.L., 1982. Cordilleran metamorphic core complexes - from Arizona to southern Canada. Annu. Rev. Earth Planet Sci. 10, 129–154.
Askvik, H., 1971. Gabbroic and Quartz Dioritic Intrusions in Gneisses on Southern Askoy, West Norwegian Caledonides, vol. 270. Norges Geologiske Undersøkelse, pp. 3–38.
Aslin, J., Mariani, E., Dawson, K., Barsoum, M.W., 2019. Ripplocations provide a new mechanism for the deformation of phyllosilicates in the lithosphere. Nat. Commun. 10, 686.
Austrheim, H., 1987. Eclogitization of lower crustal granulites by fluid migration through shear zones. Earth Planet Sci. Lett. 81, 221–232.
Austrheim, H., 2013. Fluid and deformation induced metamorphic processes around Moho beneath continent collision zones: examples from the exposed root zone of the Caledonian mountain belt, W-Norway. Tectonophysics 609, 620–635.
Austrheim, H., Ragnhildstveit, J., 1999. Berggrunnskart Herdla 1116-3 M 1:50.000. Norges geologiske undersøkelse.
Axen, G.J., 2007. Research Focus: significance of large-displacement, low-angle normal faults. Geology 35, 287–288.
Beaumont, C., Jamieson, R.A., Nguyen, M.H., Lee, B., 2001. Himalayan tectonics explained by extrusion of a low-viscosity crustal channel coupled to focused surface denudation. Nature 414, 738–742.
Bering, D.H., 1985. Tektonometamorf Utvikling Av Det Vestlige Gneiskompleks I Sund. University of Bergen, Sotra, p. 367.
Bering, D.H., Rykkelid, E., Fossen, H., 1988. Berggrunnskart Marstein 1115-3 M 1: 50.000. Norges geologiske undersøkelse.
Bernhard, J., 1994. Brittle Deformation in the Öygarden Gneiss Complex, Western Norway - Paleostress Analysis. University of Bergen, p. 113.
Bingen, B., Austrheim, H., Whitehouse, M.J., Davis, W.J., 2004. Trace element signature and U-Pb geochronology of eclogite-facies zircon, Bergen Arcs, Caledonides of W Norway. Contrib. Mineral. Petrol. 147, 671–683.
Bingen, B., Nordgulen, O., Viola, G., 2008. A four-phase model for the Sveconorwegian orogeny, SW Scandinavia. Norw. J. Geol. 88, 43–72.
Bingen, B., Skar, O., Marker, M., Sigmond, E.M.O., Nordgulen, O., Ragnhildstveit, J., Mansfeld, J., Tucker, R.D., Liegeois, J.P., 2005. Timing of continental building in the Sveconorwegian orogen, SW Scandinavia. Norw. J. Geol. 85, 87–116.
Bingen, B., Solli, A., 2009. Geochronology of magmatism in the Caledonian and Sveconorwegian belts of Baltica: synopsis for detrital zircon provenance studies. Norw. J. Geol. 89, 267–290.
Bos, B., Spiers, C.J., 2002. Frictional-viscous flow of phyllosilicate-bearing fault rock: microphysical model and implications for crustal strength profiles. J Geophys Res-Sol Ea 107, 1–13. ECV 1-1–ECV.
Boundy, T.M., Essene, E.J., Hall, C.M., Austrheim, H., Halliday, A.N., 1996. Rapid exhumation of lower crust during continent-continent collision and late extension: evidence from Ar-40/Ar-39 incremental heating of hornblendes and muscovites, Caledonian orogen, western Norway. Geol. Soc. Am. Bull. 108, 1425–1437.
Braathen, A., Nordgulen, O., Osmundsen, P.T., Andersen, T.B., Solli, A., Roberts, D., 2000. Devonian, orogen-parallel, opposed extension in the Central Norwegian Caledonides. Geology 28, 615–618.
Braathen, A., Osmundsen, P.T., Gabrielsen, R.H., 2004. Dynamic development of fault rocks in a crustal-scale detachment: an example from western Norway. Tectonics 23, 1–21.
Brun, J.-P., Sokoutis, D., Tirel, C., Gueydan, F., Van Den Driessche, J., Beslier, M.-O., 2018. Crustal versus mantle core complexes. Tectonophysics 746, 22–45.
Brun, J.P., Sokoutis, D., Van den Driessche, J., 1994. Analog modeling of detachment fault systems and core complexes. Geology 22, 319–322.
Brun, J.P., Van den Driessche, J., 1994. Extensional gneiss domes and detachment fault systems - structure and kinematics. B Soc Geol Fr 165, 519–530.
Buck, W.R., 1988. Flexural rotation of normal faults. Tectonics 7, 959–973.
Buck, W.R., 1991. Modes of continental lithospheric extension. J Geophys Res-Sol Ea 96, 20161–20178.
Burchfiel, B.C., Royden, L.H., 1985. North-south extension within the convergent Himalayan region. Geology 13, 679–682.
Butler, J.P., Beaumont, C., Jamieson, R.A., 2015. Paradigm lost: buoyancy thwarted by the strength of the Western Gneiss Region (ultra) high-pressure terrane. Norway. Lithosphere 7, 379–407.
Butler, J.P., Jamieson, R.A., Steenkamp, H.M., Robinson, P., 2013. Discovery of coesite–eclogite from the Nordøyane UHP domain, Western Gneiss Region, Norway: field relations, metamorphic history, and tectonic significance. J. Metamorph. Geol. 31, 147–163.
Cao, S., Neubauer, F., Bernroider, M., Genser, J., Liu, J., Friedl, G., 2017. Low-grade retrogression of a high-temperature metamorphic core complex: Naxos, Cyclades, Greece. GSA Bulletin 129, 93–117.
Cao, S., Neubauer, F., Bernroider, M., Liu, J., 2013. The lateral boundary of a metamorphic core complex: the Moutsounas shear zone on Naxos, Cyclades, Greece. J. Struct. Geol. 54, 103–128.
Chauvet, A., Dallmeyer, R.D., 1992. 40Ar/39Ar mineral dates related to Devonian extension in the southwestern Scandinavian Caledonides. Tectonophysics 210, 155–177.
Chauvet, A., Seranne, M., 1994. Extension-parallel folding in the scandinavian Caledonides - implications for late-orogenic processes. Tectonophysics 238, 31–54.
Clerc, C., Ringenbach, J.-C., Jolivet, L., Ballard, J.-F., 2018. Rifted margins: ductile deformation, boudinage, continentward-dipping normal faults and the role of the weak lower crust. Gondwana Res. 53, 20–40.
Coint, N., Slagstad, T., Roberts, N.M.W., Marker, M., Rohr, T., Sorensen, B.E., 2015. The late mesoproterozoic sirdal magmatic belt, SW Norway: relationships between magmatism and metamorphism and implications for sveconorwegian orogenesis. Precambrian Res. 265, 57–77.

Collettini, C., Niemeijer, A., Viti, C., Marone, C., 2009a. Fault zone fabric and fault weakness. Nature 462, 907.
Collettini, C., Viti, C., Smith, S.A.F., Holdsworth, R.E., 2009b. Development of interconnected talc networks and weakening of continental low-angle normal faults. Geology 37, 567–570.
Coney, P.J., 1980. Cordilleran metamorphic core complexes: an overview. Geol. Soc. Am. Mem. 153, 7–31.
Cooper, F.J., Platt, J.P., Behr, W.M., 2017. Rheological transitions in the middle crust: insights from Cordilleran metamorphic core complexes. Solid Earth 8, 199–215.
Cooper, F.J., Platt, J.P., Platzman, E.S., Grove, M.J., Seward, G., 2010. Opposing shear senses in a subdetachment mylonite zone: implications for core complex mechanics. Tectonics 29.
Corfu, F., Andersen, T., Gasser, D., 2014. The Scandinavian Caledonides: Main Features, Conceptual Advances and Critical Questions, vol. 390. Geological Society, London, pp. 9–43. Special Publications.
Cuthbert, S.J., Carswell, D.A., Krogh-Ravna, E.J., Wain, A., 2000. Eclogites and eclogites in the western gneiss region, Norwegian Caledonides. Lithos 52, 165–195.
Dobrzhinetskaya, L.F., Eide, E.A., Larsen, R.B., Sturt, B.A., Trønnes, R.G., Smith, D.C., Taylor, W.R., Posukhova, T.V., 1995. Microdiamond in high-grade metamorphic rocks of the Western Gneiss region. Norway. Geology 23, 597–600.
Duretz, T., Gerya, T.V., Kaus, B.J.P., Andersen, T.B., 2012. Thermomechanical modeling of slab eduction. J. Geophys. Res.: Solid Earth 117, 1–21.
Faerseth, R.B., Gjelberg, J., Martinsen, O.J., 2011. Structural geology and sedimentology of silurian metasediments in the ulven area, major Bergen Arc, SW Norway. Norw. J. Geol. 91, 19–33.
Fauconnier, J., Labrousse, L., Andersen, T.B., Beyssac, O., Duprat-Oualid, S., Yamato, P., 2014. Thermal structure of a major crustal shear zone, the basal thrust in the Scandinavian Caledonides. Earth Planet Sci. Lett. 385, 162–171.
Fazlikhani, H., Fossen, H., Gawthorpe, R.L., Faleide, J.I., Bell, R.E., 2017. Basement structure and its influence on the structural configuration of the northern North Sea rift. Tectonics 36, 1151–1177.
Fossen, H., 1988. The ulriken gneiss complex and the rundemanen formation: a basement-cover relationship in the bergen arcs, west Norway. Nor. Geol. Unders. Bull. 412, 67–86.
Fossen, H., 1989. Geology of the minor Bergen Arc, west Norway. Nor. Geol. Unders. Bull. 416, 47–62.
Fossen, H., 1992. The role of extensional tectonics in the Caledonides of south Norway. J. Struct. Geol. 14, 1033–1046.
Fossen, H., 1998. Advances in understanding the post-Caledonian structural evolution of the Bergen Area, West Norway. Nor. Geol. Tidsskr. 78, 33–46.
Fossen, H., 2000. Extensional tectonics in the Caledonides: synorogenic or postorogenic? Tectonics 19, 213–224.
Fossen, H., 2010. Extensional Tectonics in the North Atlantic Caledonides: a Regional View, vol. 335. Geological Society, London, pp. 767–793. Special Publications.
Fossen, H., 2016. Structural Geology, second ed. Cambridge University Press.
Fossen, H., Cavalcante, G.C., de Almeida, R.P., 2017. Hot versus cold orogenic behavior: comparing the araçuaí-west Congo and the caledonian orogens. Tectonics 36, 2159–2178.
Fossen, H., Dallmeyer, R.D., 1998. Ar-40/Ar-39 muscovite dates from the nappe region of southwestern Norway: dating extensional deformation in the Scandinavian Caledonides. Tectonophysics 285, 119–133.
Fossen, H., Dunlap, W.J., 1998. Timing and kinematics of Caledonian thrusting and extensional collapse, southern Norway: evidence from Ar-40/Ar-39 thermochronology. J. Struct. Geol. 20, 765–781.
Fossen, H., Dunlap, W.J., 1999. On the age and tectonic significance of Permo-Triassic dikes in the Bergen-Sunnhordland region, southwestern Norway. Nor. Geol. Tidsskr. 79, 169–178.
Fossen, H., Dunlap, W.J., 2006. Age constraints on the late caledonian (scandian) deformation in the major Bergen Arc, SW Norway. Norw. J. Geol. 86, 59–70.
Fossen, H., Fazlikhani, H., Faleide, J.I., Ksienzyk, A.K., Dunlap, W.J., 2016. Post-caledonian Extension in the West Norway–northern North Sea Region: the Role of Structural Inheritance, vol. 439. Geological Society, London, pp. 465–486. Special Publications.
Fossen, H., Gabrielsen, R.H., Faleide, J.I., Hurich, C.A., 2014. Crustal stretching in the Scandinavian Caledonides as revealed by deep seismic data. Geology 42, 791–794.
Fossen, H., Hurich, C.A., 2005. The hardangerfjord shear zone in SW Norway and the north sea: a large-scale low-angle shear zone in the caledonian crust. J. Geol. Soc. 162, 675–687.
Fossen, H., Ragnhildstveit, J., 2008. Berggrunnskart Bergen 1115 I, M 1:50.000. Norges Geologiske Undersøkelse.
Fossen, H., Rykkelid, E., 1990. Shear zone structures in the oygarden area, west Norway. Tectonophysics 174, 385–397.
Fossen, H., Rykkelid, E., 1992. The interaction between oblique and layer-parallel shear in high-strain zones - observations and experiments. Tectonophysics 207, 331–343.
Fossen, H., Teyssier, C., Whitney, D.L., 2013. Transtensional folding. J. Struct. Geol. 56, 89–102.
Furnes, H., Dilek, Y., Pedersen, R.B., 2012. Structure, geochemistry, and tectonic evolution of trench-distal backarc oceanic crust in the western Norwegian Caledonides, Solund-Stavfjord ophiolite (Norway). Geol. Soc. Am. Bull. 124, 1027–1047.
Fusseis, F., Regenauer-Lieb, K., Liu, J., Hough, R.M., De Carlo, F., 2009. Creep cavitation can establish a dynamic granular fluid pump in ductile shear zones. Nature 459, 974–977.
Ganzhorn, A.C., Labrousse, L., Prouteau, G., Leroy, C., Vrijmoed, J.C., Andersen, T.B., Arbaret, L., 2014. Structural, petrological and chemical analysis of syn-kinematic migmatites: insights from the Western Gneiss Region, Norway. J. Metamorph. Geol. 32, 647–673.
Gee, D.G., Fossen, H., Henriksen, N., Higgins, A.K., 2008. From the early paleozoic platforms of Baltica and Laurentia to the caledonide orogen of scandinavia and Greenland. Episodes 31, 44–51.
Gellein, J., 2007a. Aeromagnetisk Anomalikart, vol. 1. Norges geologiske undersøkelse, Bergen, p. 250, 000.
Gellein, J., 2007b. Gravimetrisk Residualkart, vol. 1. Norges geologiske undersøkelse, Bergen, p. 250, 000.
Gordon, S.M., Whitney, D.L., Teyssier, C., Fossen, H., 2013. U-Pb dates and trace-element geochemistry of zircon from migmatite, Western Gneiss Region, Norway: significance for history of partial melting in continental subduction. Lithos 170, 35–53.
Gordon, S.M., Whitney, D.L., Teyssier, C., Fossen, H., Kylander-Clark, A., 2016. Geochronology and geochemistry of zircon from the northern Western Gneiss Region: insights into the Caledonian tectonic history of western Norway. Lithos 246–247, 134–148.
Grasemann, B., Tschegg, C., 2012. Localization of deformation triggered by chemo-mechanical feedback processes. GSA Bulletin 124, 737–745.
Griffin, W.L., Brueckner, H.K., 1980. Caledonian Sm–Nd ages and a crustal origin for Norwegian eclogites. Nature 285, 319–321.
Grujic, D., 2006. Channel Flow and Continental Collision Tectonics: an Overview, vol. 268. Geological Society, London, pp. 25–37. Special Publications.
Grujic, D., Casey, M., Davidson, C., Hollister, L.S., Kündig, R., Pavlis, T., Schmid, S., 1996. Ductile extrusion of the Higher Himalayan Crystalline in Bhutan: evidence from quartz microfabrics. Tectonophysics 260, 21–43.
Grünwald, R., 1994. Faulted Basement in Westernmost Onshore Norway (Øygarden) and its Offshore Seismic Image. University of Bergen, p. 135.
Hacker, B.R., Abers, G.A., Peacock, S.M., 2003a. Subduction factory 1. Theoretical mineralogy, densities, seismic wave speeds, and H2O contents. J. Geophys. Res.: Solid Earth 108.
Hacker, B.R., Andersen, T.B., Johnston, S., Kylander-Clark, A.R.C., Peterman, E.M., Walsh, E.O., Young, D., 2010. High-temperature deformation during continental-margin subduction & exhumation: the ultrahigh-pressure Western Gneiss Region of Norway. Tectonophysics 480, 149–171.
Hacker, B.R., Andersen, T.B., Root, D.B., Mehl, L., Mattinson, J.M., Wooden, J.L., 2003b. Exhumation of high-pressure rocks beneath the solund basin, western gneiss region of Norway. J. Metamorph. Geol. 21, 613–629.
Hartz, E.H., Andresen, A., Hodges, K.V., Martin, M.W., 2001. Syncontractional extension and exhumation of deep crustal rocks in the east Greenland Caledonides. Tectonics 20, 58–77.
Hirth, G., Tullis, J., 1992. Dislocation creep regimes in quartz aggregates. J. Struct. Geol. 14, 145–159.
Hodges, K.V., 2016. Crustal decoupling in collisional orogenesis: examples from the east Greenland Caledonides and himalaya. Annu. Rev. Earth Planet Sci. 44, 685–708.
Holdsworth, R.E., 2004. Weak faults–rotten cores. Science 303, 181–182.
Holtedahl, H., 1998. The Norwegian strandflat-a geomorphological puzzle. Nor. Geol. Tidsskr. 78, 47–66.
Hossack, J.R., 1984. The geometry of listric growth faults in the Devonian basins of Sunnfjord, W Norway. J. Geol. Soc. 141, 629–637.
Huet, B., Le Pourhiet, L., Labrousse, L., Burov, E., Jolivet, L., 2011. Post-orogenic extension and metamorphic core complexes in a heterogeneous crust: the role of crustal layering inherited from collision. Application to the Cyclades (Aegean domain). Geophys. J. Int. 184, 611–625.
Hunter, N.J.R., Hasalová, P., Weinberg, R.F., Wilson, C.J.L., 2016. Fabric controls on strain accommodation in naturally deformed mylonites: the influence of interconnected micaceous layers. J. Struct. Geol. 83, 180–193.
Jakob, J., Alsaif, M., Corfu, F., Andersen, T.B., 2017. Age and origin of thin discontinuous gneiss sheets in the distal domain of the magma-poor hyperextended pre-Caledonian margin of Baltica, southern Norway. J. Geol. Soc. 174, 557–571.
Jakob, J., Andersen, T.B., Kjøll, H.J., 2019. A review and reinterpretation of the architecture of the South and South-Central Scandinavian Caledonides—a magma-poor to magma-rich transition and the significance of the reactivation of rift inherited structures. Earth Sci. Rev. 192, 513–528.
John, B.E., Cheadle, M.J., 2013. Deformation and alteration associated with oceanic and continental detachment fault systems: are they similar? In: Rona, P.A., D, C.W., Dyment, J., Murton, B.J. (Eds.), Diversity of Hydrothermal Systems on Slow Spreading Ocean Ridges. American Geophysical Union, pp. 175–205.
Johns, C.C., 1981. The geology of northern Sotra: precambrian gneisses west of the bergen arcs, Norway. Bedford College. University of London, p. 397.
Johns, C.C., Ragnhildstveit, J., Bering, D.H., 2001. Berggrunnskart FJELL 1116-3 M 1: 50.000. Norges geologiske undersøkelse.
Johnston, S., Hacker, B.R., Ducea, M.N., 2007a. Exhumation of ultrahigh-pressure rocks beneath the hornelen segment of the nordfjord-sogn detachment zone, western Norway. GSA Bulletin 119, 1232–1248.
Johnston, S.M., Hacker, B.R., Andersen, T.B., 2007b. Exhuming Norwegian ultrahigh-pressure rocks: overprinting extensional structures and the role of the Nordfjord-Sogn Detachment Zone. Tectonics 26, 1–12.
Jolivet, L., Brun, J.-P., 2010. Cenozoic geodynamic evolution of the Aegean. Int. J. Earth Sci. 99, 109–138.
Jolivet, L., Famin, V., Mehl, C., Parra, T., Aubourg, C., Hebert, R., Philippot, P., 2004. Strain localization during crustal-scale boudinage to form extensional metamorphic domes in the Aegean Sea. Geol. Soc. Am. Spec. Pap. 380, 185–210.
Jolivet, L., Menant, A., Clerc, C., Sternai, P., Bellahsen, N., Leroy, S., Pik, R., Stab, M., Faccenna, C., Gorini, C., 2018. Extensional crustal tectonics and crust-mantle coupling, a view from the geological record. Earth Sci. Rev. 185, 1187–1209.

Jolivet, L., Raimbourg, H., Labrousse, L., Avigad, D., Leroy, Y., Austrheim, H., Andersen, T.B., 2005. Softening trigerred by eclogitization, the first step toward exhumation during continental subduction. Earth Planet Sci. Lett. 237, 532–547.
Kjøll, H.J., Andersen, T.B., Corfu, F., Labrousse, L., Tegner, C., Abdelmalak, M.M., Planke, S., 2019. Timing of breakup and thermal evolution of a pre-caledonian neoproterozoic exhumed magma-rich rifted margin. Tectonics 38, 1843–1862.
Kleine, B.I., Pitcairn, I.K., Skelton, A.D.L., 2015. The mechanism of infiltration of metamorphic fluids recorded by hydration and carbonation of epidote-amphibolite facies metabasaltic sills in the SW Scottish Highlands†. Am. Mineral. 100, 2702–2717.
Kolderup, C.F., Kolderup, N.H., 1940. Geology of the Bergen Arc System. Bergen Museum, Bergen.
Krabbendam, M., Dewey, J.F., 1998. Exhumation of UHP Rocks by Transtension in the Western Gneiss Region, Scandinavian Caledonides, vol. 135. Geological Society, London, pp. 159–181. Special Publications.
Kruckenberg, S.C., Vanderhaeghe, O., Ferre, E.C., Teyssier, C., Whitney, D.L., 2011. Flow of partially molten crust and the internal dynamics of a migmatite dome, Naxos, Greece. Tectonics 30.
Ksienzyk, A.K., Dunkl, I., Jacobs, J., Fossen, H., Kohlmann, F., 2014. From Orogen to Passive Margin: Constraints from Fission Track and (U–Th)/He Analyses on Mesozoic Uplift and Fault Reactivation in SW Norway, vol. 390. Geological Society, London, pp. 679–702. Special Publications.
Ksienzyk, A.K., Wemmer, K., Jacobs, J., Fossen, H., Schomberg, A.C., Sussenberger, A., Lunsdorf, N.K., Bastesen, E., 2016. Post-Caledonian brittle deformation in the Bergen area, West Norway: results from K-Ar illite fault gouge dating. Norw. J. Geol. 96, 275–299.
Kuhn, A., Glodny, J., Austrheim, H., Raheim, A., 2002. The Caledonian tectono-metamorphic evolution of the Lindas Nappe: constraints from U-Pb, Sm-Nd and Rb-Sr ages of granitoid dykes. Norw. J. Geol. 82, 45–57.
Kvale, A., 1960. The Nappe Area of the Caledonides in Western Norway, vol. 212e. Norges Geologiske Undersøkelse Bulletin, pp. 21–43.
Kylander-Clark, A.R.C., Hacker, B.R., 2014. Age and significance of felsic dikes from the UHP western gneiss region. Tectonics 33, 2342–2360.
Kylander-Clark, A.R.C., Hacker, B.R., Mattinson, J.M., 2008. Slow exhumation of UHP terranes: titanite and rutile ages of the western gneiss region, Norway. Earth Planet Sci. Lett. 272, 531–540.
Labrousse, L., Hetényi, G., Raimbourg, H., Jolivet, L., Andersen, T.B., 2010. Initiation of crustal-scale thrusts triggered by metamorphic reactions at depth: insights from a comparison between the Himalayas and Scandinavian Caledonides. Tectonics 29, 1–14.
Labrousse, L., Huet, B., Le Pourhiet, L., Jolivet, L., Burov, E., 2016. Rheological implications of extensional detachments: mediterranean and numerical insights. Earth Sci. Rev. 161, 233–258.
Labrousse, L., Jolivet, L., Agard, P., Hebert, R., Andersen, T.B., 2002. Crustal-scale boudinage and migmatization of gneiss during their exhumation in the UHP Province of Western Norway. Terra. Nova 14, 263–270.
Labrousse, L., Jolivet, L., Andersen, T., Agard, P., Hébert, R., Maluski, H., Schärer, U., 2004. Pressure-temperature-time deformation history of the exhumation of ultra-high pressure rocks in the Western Gneiss Region, Norway. Geol. Soc. Am. Spec. Pap. 380, 155–183.
Labrousse, L., Prouteau, G., Ganzhorn, A.-C., 2011. Continental exhumation triggered by partial melting at ultrahigh pressure. Geology 39, 1171–1174.
Larsen, O., 1996. Fedjedomens tektoniske utvikling (Øygarden gneiskompleks, vest Norge) - en alternative model for dannelse av gneisdomer. University of Bergen, p. 155.
Larsen, O., Fossen, H., Langeland, K., Pedersen, R.B., 2003. Kinematics and timing of polyphase post-Caledonian deformation in the Bergen area, SW Norway. Norw. J. Geol. 83, 149–165.
Lavier, L.L., Buck, W.R., 2002. Half graben versus large-offset low-angle normal fault: importance of keeping cool during normal faulting. J. Geophys. Res.: Solid Earth 107, 8–13. ETG 8-1-ETG.
Lavier, L.L., Buck, W.R., Poliakov, A.N.B., 1999. Self-consistent rolling-hinge model for the evolution of large-offset low-angle normal faults. Geology 27, 1127–1130.
Le Pourhiet, L., Huet, B., May, D.A., Labrousse, L., Jolivet, L., 2012. Kinematic interpretation of the 3D shapes of metamorphic core complexes. G-cubed 13, 1–17.
Lenhart, A., Jackson, C.A.-L., Bell, R.E., Duffy, O.B., Gawthorpe, R.L., Fossen, H., 2019. Structural architecture and composition of crystalline basement offshore west Norway. Lithosphere 11, 273–293.
Lister, G.S., Davis, G.A., 1989. The origin of metamorphic core complexes and detachment faults formed during tertiary continental extension in the northern Colorado river region, USA. J. Struct. Geol. 11, 65–94.
McClay, Norton, M, G., Coney, P., Davis, G.H., 1986. Collapse of the caledonian orogen and the old red sandstone. Nature 323, 147–149.
Miller, E.L., Dumitru, T.A., Brown, R.W., Gans, P.B., 1999. Rapid miocene slip on the snake range–deep creek range fault system, east-central Nevada. GSA Bulletin 111, 886–905.
Milnes, A., Wennberg, O., Skår, Ø., Koestler, A., 1997. Contraction, Extension and Timing in the South Norwegian Caledonides: the Sognefjord Transect, vol. 121. Geological Society, London, pp. 123–148. Special Publications.
Norlander, B.H., Whitney, D.L., Teyssier, C., Vanderhaeghe, O., 2002. Partial melting and decompression of the Thor-Odin dome, Shuswap metamorphic core complex, Canadian Cordillera. Lithos 61, 103–125.
Norton, M.G., 1987. The nordfjord-sogn detachment, W Norway. Nor. Geol. Tidsskr. 67, 93–106.
Osmundsen, P.T., Andersen, T.B., 2001. The middle Devonian basins of western Norway: sedimentary response to large-scale transtensional tectonics? Tectonophysics 332, 51–68.
Osmundsen, P.T., Braathen, A., Sommaruga, A., Skilbrei, J.R., Nordgulen, O., Roberts, D., Andersen, T.B., Olesen, O., Mosar, J., 2005. Metamorphic core complexes and gneiss-cored culminations along the Mid-Norwegian margin: an overview and some current ideas. Norwegian Petroleum Society Special Publications 12, 29–41.
Osmundsen, P.T., Eide, E.A., Haabesland, N.E., Roberts, D., Andersen, T.B., Kendrick, M., Bingen, B., Braathen, A., Redfield, T.F., 2006. Kinematics of the høybakken detachment zone and the møre–trøndelag fault complex, central Norway. J. Geol. Soc. 163, 303–318.
Osmundsen, P.T., Péron-Pinvidic, G., 2018. Crustal-scale fault interaction at rifted margins and the formation of domain-bounding breakaway complexes: insights from offshore Norway. Tectonics 37, 935–964.
Pascal, C., Rudlang, T., 2016. Discovery of highly radioactive granite in the Bergen Region. Norw. J. Geol. 96, 319–328.
Pedersen, R.B., Bruton, D.L., Furnes, H., 1992. Ordovician faunas, island arcs and ophiolites in the scandinavian Caledonides. Terra. Nova 4, 217–222.
Pennacchioni, G., Mancktelow, N.S., 2007. Nucleation and initial growth of a shear zone network within compositionally and structurally heterogeneous granitoids under amphibolite facies conditions. J. Struct. Geol. 29, 1757–1780.
Platt, J.P., Behr, W.M., Cooper, F.J., 2015. Metamorphic core complexes: windows into the mechanics and rheology of the crust. J. Geol. Soc. 172, 9–27.
Quilichini, A., Siebenaller, L., Teyssier, C., Vennemann, T.W., 2016. Magmatic and meteoric fluid flow in the Bitterroot extensional detachment shear zone (MT, USA) from ductile to brittle conditions. J. Geodyn. 101, 109–128.
Ragnhildstveit, J., Helliksen, D., 1997. Geologisk Kart over Norge, Berggrunnskart Bergen - M 1:250.000. Norges Geologiske Undersøkelse.
Rey, P., Burg, J.-P., Casey, M., 1997. The scandinavian Caledonides and their relationship to the variscan belt. Geological society, london,. Spec. Publ. 121, 179–200.
Rey, P., Vanderhaeghe, O., Teyssier, C., 2001. Gravitational collapse of the continental crust: definition, regimes and modes. Tectonophysics 342, 435–449.
Rey, P.F., Mondy, L., Duclaux, G., Teyssier, C., Whitney, D.L., Bocher, M., Prigent, C., 2017. The origin of contractional structures in extensional gneiss domes. Geology 45, 263–266.
Rey, P.F., Teyssier, C., Whitney, D.L., 2009. Extension rates, crustal melting, and core complex dynamics. Geology 37, 391–394.
Roberts, N.M.W., Slagstad, T., 2015. Continental growth and reworking on the edge of the Columbia and Rodinia supercontinents; 1.86-0.9 Ga accretionary orogeny in southwest Fennoscandia. Int. Geol. Rev. 57, 1582–1606.
Roberts, N.M.W., Slagstad, T., Parrish, R.R., Norry, M.J., Marker, M., Horstwood, M.S.A., 2013. Sedimentary recycling in arc magmas: geochemical and U-Pb-Hf-O constraints on the Mesoproterozoic Suldal Arc, SW Norway. Contrib. Mineral. Petrol. 165, 507–523.
Roger, F., Teyssier, C., Respaut, J.P., Rey, P.F., Jolivet, M., Whitney, D.L., Paquette, J.L., Brunel, M., 2015. Timing of formation and exhumation of the Montagne Noire double dome, French massif central. Tectonophysics 640, 53–69.
Root, D.B., Hacker, B.R., Gans, P.B., Ducea, M.N., Eide, E.A., Mosenfelder, J.L., 2005. Discrete ultrahigh-pressure domains in the Western Gneiss Region, Norway: implications for formation and exhumation. J. Metamorph. Geol. 23, 45–61.
Rosenberg, C.L., Handy, M.R., 2005. Experimental deformation of partially melted granite revisited: implications for the continental crust. J. Metamorph. Geol. 23, 19–28.
Rudlang, T., 2011. Heat flow and deep underground temperature in the bergen region. MSc Thesis NTNU Trondheim, 75 p.
Rykkelid, E., Fossen, H., 1992. Composite fabrics in midcrustal gneisses - observations from the oygarden complex, west Norway Caledonides. J. Struct. Geol. 14, 1–9.
Scheiber, T., Viola, G., Wilkinson, C.M., Ganerød, M., Skår, Ø., Gasser, D., 2016. Direct 40Ar/39Ar dating of late ordovician and silurian brittle faulting in the southwestern Norwegian Caledonides. Terra. Nova 28, 374–382.
Schulze, K., 2014. Radiogenic Heat Production in the Bed Rock of Bergen, Norway with Gamma-Spectrometry and its Relevance for Geothermal Energy. MSc thesis. Christian-Albrechts Universität Kiel, p. 108.
Searle, M.P., 2010. Low-angle normal faults in the compressional himalayan orogen; evidence from the annapurna–dhaulagiri himalaya, Nepal. Geosphere 6, 296–315.
Searle, M.P., Lamont, T.N., 2020. Compressional metamorphic core complexes, low-angle normal faults and extensional fabrics in compressional tectonic settings. Geol. Mag. 157, 101–118.
Séguret, M., Séranne, M., Chauvet, A., Brunel, A., 1989. Collapse basin: a new type of extensional sedimentary basin from the Devonian of Norway. Geology 17, 127–130.
Seranne, M., 1992. Late palaeozoic kinematics of the møre-trøndelag fault zone and adjacent areas, central Norway. Nor. Geol. Tidsskr. 72, 141–158.
Seranne, M., Seguret, M., 1987. The Devonian Basins of Western Norway: Tectonics and Kinematics of an Extending Crust, vol. 28. Geological Society, London, pp. 537–548. Special Publications.
Siebenaller, L., Boiron, M.C., Vanderhaeghe, O., Hibsch, C., Jessell, M.W., Andre-Mayer, A.S., France-Lanord, C., Photiades, A., 2012. Fluid record of rock exhumation across the brittle–ductile transition during formation of a Metamorphic Core Complex (Naxos Island, Cyclades, Greece). J. Metamorph. Geol. 31, 313–338.
Slagstad, T., Kirkland, C.L., 2018. Timing of collision initiation and location of the Scandian orogenic suture in the Scandinavian Caledonides. Terra. Nova 30, 179–188.
Slagstad, T., Maystrenko, Y., Maupin, V., Gradmann, S., 2018a. An extinct, Late Mesoproterozoic, Sveconorwegian mantle wedge beneath SW Fennoscandia,

reflected in seismic tomography and assessed by thermal modelling. Terra. Nova 30, 72–77.
Slagstad, T., Roberts, N.M.W., Coint, N., Høy, I., Sauer, S., Kirkland, C.L., Marker, M., Røhr, T.S., Henderson, I.H.C., Stormoen, M.A., Skår, Ø., Sørensen, B.E., Bybee, G., 2018b. Magma-driven, high-grade metamorphism in the Sveconorwegian Province, southwest Norway, during the terminal stages of Fennoscandian Shield evolution. Geosphere 14, 861–882.
Slagstad, T., Roberts, N.M.W., Marker, M., Rohr, T.S., Schiellerup, H., 2013. A non-collisional, accretionary Sveconorwegian orogen. Terra. Nova 25, 30–37.
Spencer, K.J., Hacker, B.R., Kylander-Clark, A.R.C., Andersen, T.B., Cottle, J.M., Stearns, M.A., Poletti, J.E., Seward, G.G.E., 2013. Campaign-style titanite U–Pb dating by laser-ablation ICP: implications for crustal flow, phase transformations and titanite closure. Chem. Geol. 341, 84–101.
Sturt, B.A., Skarpenes, O., Ohanian, A.T., Pringle, I.R., 1975. Reconnaissance Rb-Sr isochron study in Bergen Arc system and regional implications. Nature 253, 595–599.
Teyssier, C., Ferré, E.C., Whitney, D.L., Norlander, B., Vanderhaeghe, O., Parkinson, D., 2005. Flow of Partially Molten Crust and Origin of Detachments during Collapse of the Cordilleran Orogen, vol. 245. Geological Society, London, pp. 39–64. Special Publications.
Tirel, C., Brun, J.P., Burov, E., 2008. Dynamics and structural development of metamorphic core complexes. J Geophys Res-Sol Ea 113.
Tirel, C., Brun, J.P., Sokoutis, D., 2006. Extension of thickened and hot lithospheres: inferences from laboratory modeling. Tectonics 25.
Vanderhaeghe, O., Laurent, O., Gardien, V., Moyen, J.-F., Gébelin, A., Chelle-Michou, C., Couzinié, S., Villaros, A., Bellanger, M., 2020. Flow of partially molten crust controlling construction, growth and collapse of the Variscan orogenic belt: the geologic record of the French Massif Central. BSGF-Earth Sciences Bulletin. https://doi.org/10.1051/bsgf/2020013 (Forthcoming).
Vanderhaeghe, O., Teyssier, C., McDougall, I., Dunlap, W.J., 2003. Cooling and exhumation of the Shuswap metamorphic core complex constrained by Ar-40/Ar-39 thermochronology. Geol. Soc. Am. Bull. 115, 200–216.
Vanderhaeghe, O., Teyssier, C., Wysoczanski, R., 1999. Structural and geochronological constraints on the role of partial melting during the formation of the Shuswap metamorphic core complex at the latitude of the Thor-Odin dome, British Columbia. Can. J. Earth Sci. 36, 917–943.
Vanderhaeghe, O., Whitney, D.L., Teyssier, C., Siddoway, C.S., 2004. Structural Development of the Naxos Migmatite Dome, Geol Soc Am Spec Pap. Geological Society of America, pp. 211–228.
Vannay, J.-C., Grasemann, B., 2001. Himalayan inverted metamorphism and syn-convergence extension as a consequence of a general shear extrusion. Geol. Mag. 138, 253–276.
Wain, A., 1997. New evidence for coesite in eclogite and gneisses: defining an ultrahigh-pressure province in the Western Gneiss region of Norway. Geology 25, 927–930.
Walsh, E.O., Hacker, B.R., Gans, P.B., Wong, M.S., Andersen, T.B., 2013. Crustal exhumation of the Western Gneiss Region UHP terrane, Norway: 40Ar/39Ar thermochronology and fault-slip analysis. Tectonophysics 608, 1159–1179.
Weiss, L.E., 1977. Structural Features of the Laksevåg Gneiss, vol. 334. Norges Geologiske Undersøkelse, Bergen, Norway, pp. 1–17.
Wennberg, O.P., 1996. Superimposed fabrics due to reversal of shear sense: an example from the Bergen Arc Shear Zone, western Norway. J. Struct. Geol. 18, 871–889.
Wennberg, O.P., Milnes, A.G., Winsvold, I., 1998. The northern Bergen Arc Shear Zone - an oblique-lateral ramp in the Devonian extensional detachment system of western Norway. Nor. Geol. Tidsskr. 78, 169–184.
Wernicke, B., 1981. Low-angle normal faults in the basin and range province - nappe tectonics in an extending orogen. Nature 291, 645–648.
Whitney, D.L., Roger, F., Teyssier, C., Rey, P.F., Respaut, J.P., 2015. Syn-collapse eclogite metamorphism and exhumation of deep crust in a migmatite dome: the P–T–t record of the youngest Variscan eclogite (Montagne Noire, French Massif Central). Earth Planet Sci. Lett. 430, 224–234.
Whitney, D.L., Teyssier, C., Rey, P., Buck, W.R., 2013. Continental and oceanic core complexes. Geol. Soc. Am. Bull. 125, 273–298.
Wiest, J.D., 2020. Exhumation of the Caledonian Orogenic Infrastructure in West Norway - Concepts - Structures - Ages - Reactivation. Department of Earth Science. University of Bergen, Bergen, p. 298.
Wiest, J.D., Jacobs, J., Fossen, H., Osmundsen, P.T., Ganerød, M., 2018a. Crustal Structure and Post-collisional Exhumation of the Øygarden Complex, SW Norway Caledonides, EGU General Assembly 2018. EGU, Vienna.
Wiest, J.D., Jacobs, J., Ksienzyk, A.K., Fossen, H., 2018b. Sveconorwegian vs. Caledonian orogenesis in the eastern Øygarden Complex, SW Norway – geochronology, structural constraints and tectonic implications. Precambrian Res. 305, 1–18.
Wiest, J.D., Osmundsen, P.T., Jacobs, J., Fossen, H., 2019. Deep crustal flow within post-orogenic metamorphic core complexes – insights from the southern Western Gneiss Region of Norway. Tectonics 38, 4267–4289.
Wijns, C., Weinberg, R., Gessner, K., Moresi, L., 2005. Mode of crustal extension determined by rheological layering. Earth Planet Sci. Lett. 236, 120–134.
Wintsch, R.P., Christoffersen, R., Kronenberg, A.K., 1995. Fluid-rock reaction weakening of fault zones. J Geophys Res-Sol Ea 107, 13,021–13,032.
Yin, A., 2004. Gneiss domes and gneiss dome systems. Geol. Soc. Am. Spec. Pap. 380, 1–14.
Ytredal, R.-K., 1996. Structural History of the Øygarden Gneiss Complex, Western Norway, with Special Emphasis on Late Caledonian Shear Zones. University of Bergen, p. 145.
Ytredal, T.-O., 1995. General Geology and Analysis of Brittle Structures in the Kollsnes Area, Øygarden, Western Norway: by Tor-Olav Ytredal. University of Bergen, p. 156.
Zack, T., Kooijman, E., 2017. Petrology and geochronology of rutile. Rev. Mineral. Geochem. 83, 443–467.
Zhang, J., Santosh, M., Wang, X., Guo, L., Yang, X., Zhang, B., 2012. Tectonics of the northern himalaya since the India–asia collision. Gondwana Res. 21, 939–960.